Protein Cytoplasmic Delivery using Polyampholyte Nanoparticles and Freeze Concentration

Sana Ahmed[1,2], Fumiaki Hayashi[3], Toshio Nagashima[4], and Kazuaki Matsumura[1*]

1. School of Materials Science, Japan Advanced Institute of Science and Technology, 1-1 Asahidai, Nomi, Ishikawa 923-1292, Japan

2. M. Tech (CSPT), Department of Chemistry, University of Delhi, Delhi-110007, India

3. NMR Facility Support Unit, NMR Facility, Division of Structural and Synthetic Biology, RIKEN Center for Life Science Technologies, 1-7-22 Suehiro-cho, Tsurumi-ku, Yokohama City, Kanagawa, 230-0045, Japan

4. NMR Facility, Division of Structural and Synthetic Biology, RIKEN Center for Life Science Technologies, 1-7-22 Suehiro-cho, Tsurumi-ku, Yokohama City, Kanagawa, 230-0045, Japan

*To whom correspondence should be addressed: Kazuaki Matsumura

E-mail: mkazuaki@jaist.ac.jp

Tel: +81-761-51-1680

Fax: +81-761-51-1149

ABSTRACT

A protein delivery method using freeze concentration was presented with a variety of polyampholyte nanocarriers. In order to develop protein nanocarriers, hydrophobically modified polyampholytes were synthesized by the succinylation of ε-poly-L-lysine with dodecyl succinic anhydride and succinic anhydride. The self-assembled polyampholyte aggregated form nanoparticles through intermolecular hydrophobic and electrostatic interactions when dissolved in aqueous media. The cationic and anionic nanoparticles were easily prepared by changing the succinylation ratio. Anionic or cationic proteins were adsorbed on/into the nanoparticles depending on their surface charges. The protein-loaded nanoparticles were stable for at least 7 d. When L929 cells were frozen with the protein-loaded nanoparticles in the presence of a cryoprotectant, the adsorption of the protein-loaded nanoparticles was enhanced and can be explained by the freeze concentration mechanism. After thawing, proteins were internalized into cells via endocytosis. This was the first report that showed that the efficacy of protein delivery was successfully enhanced by the freeze concentration method. This method could be useful for in vitro cytoplasmic protein or peptide delivery to various cells for immunotherapy or phenotype transformations.

Keywords: protein delivery, freeze concentration, polyampholytes, nanoparticles

1. Introduction

Over the past few decades, a significant amount of progress has been made regarding drug delivery technologies, which have engendered biomaterials for the intracellular and endocytic delivery of various therapeutic agents [1]. Examples of carriers include polymeric micelles [2-4], liposomes [5-7], microparticles [8], nanoparticles [9-11], nanogels [12,13], drug polymer conjugates [14], inorganic conjugations [15], and other supramolecular assemblies [16]. However, challenges such as low specific targeting, insufficient cellular uptake, and low therapeutic efficiency still exist in regard to the delivery of clinically optimal levels of therapeutic molecules [17]. There is a great need for the development of approaches that can transport drugs precisely and safely to a target site with a controlled release to achieve the maximum therapeutic effect [18]. Currently, nanocarriers are promising vehicles with highly improved pharmacokinetics [19], biodistributions, and toxicities, and they exhibit a number of other attractive features [13]. The intracellular delivery of proteins and peptides to living cells offers a powerful alternative to gene or siRNA transfections [20]. For such technology to be successful, the delivered protein needs to cross the plasma membrane to be efficiently released in the cytoplasm [21]. Methods such as electroporation, microinjection, or macromolecular systems have been adapted to introduce proteins into cells by penetrating cell membranes. Although the ability to introduce proteins into the cytoplasm of live cells was facilitated by the development of delivery reagents, the efficiency of the process remains low. Therefore, there is a pressing need to develop a novel method to enhance the intracellular uptake of drugs. Here, we propose an effective method using the “freeze concentration” mechanism [22-24].

Freezing is commonly believed to be the best method for long-term cell preservation. During freezing, ice can form in the extracellular space. The formation of ice can exclude solute molecules, leading to increased concentrations of electrolytes in the remaining

extracellular solution via phase separation. The phenomenon is called freeze concentration [22]. Intracellular water can remain in a super-cooled unfrozen state, even at temperatures between -5 and -40 ^{o}C. The growing extracellular ice forms channels where the extracellular solution and the cells are displaced. In these channels, the target drug also can be concentrated around the cell membranes, and its adsorption might be enhanced if the drug molecules are encapsulated with cytocompatible carriers.

In order to improve the survival of cryopreseved cells, cryoprotective agents (CPAs) like dimethyl sulfoxide (DMSO), glycerol, and ethylene glycol are often utilized. The effects of CPAs are determined by their ability to reduce the freezing and thawing points, and to lower the cooling rate to avoid lethal intracellular freezing.

Previously, we developed a cryoprotectant as an alternative to DMSO. Cells were successfully cryopreserved using poly-L-lysine (PLL) reacted with succinic anhydride at an appropriate polyampholyte ratio [24-27]. The polyampholytes effected their cryoprotective properties by a different mechanism than DMSO, and the mechanism might be related to the control of freeze concentration. We attempted to use the freeze concentration method with polyampholytes by utilizing an enhanced concentration of peripheral solutes for the introduction of antigenic proteins into the cytosol of cells as an effective immunotherapy [28].

Cytocompatible nanocarriers have been widely studied. Moreover, many researchers have shown that polymer-peptide conjugates form self-assembled nanostructures based on the interactions of well-defined amino acid residues [29,30]. Polyampholytes have also gained great attention in various areas such as biotechnology, and have a promising future in the delivery of diagnostic agents. For example, Akashi and co-researchers reported amphoteric poly(amino acid) nanoparticles for protein delivery [31].

Here, we describe the development of a facile and effective protein delivery method to address the issues of inefficient cellular uptake and poor intracellular protein behaviors of protein-loaded nanoparticles using the freeze concentration mechanism and amphoteric

nanocarriers. Specifically, nanoparticles formed by the self-assembly of amphiphilic charged polyampholytes containing extensive cross-linking points showed a high drug trapping efficiency. Nanoparticles were characterized by particle size, zeta potential, and morphological observation and interacted via hydrophobic and electrostatic interactions.

2. Experimental Section

2.1 Preparation of polyampholytes and hydrophobically modified polyampholytes

Polyampholyte cryoprotectants were synthesized using a previously reported method [24]. Briefly, an aqueous solution of 25 % (w/w) PLL (10 mL, JNC Corp., Tokyo, Japan) and succinic anhydride (SA) (1.3 g; Wako Pure Chem. Ind. Ltd., Osaka Japan) were mixed at 50 ^{o}C for 2 h to convert 65 % of the amino groups to carboxyl groups.

To develop polyampholyte nanoparticles, hydrophobic moieties were introduced on the polyampholyte. An aqueous solution of PLL (10 mL; 25 % w/w) was added to different concentrations of dodecyl succinic anhydride (DDSA) (Wako Pure Chem. Ind. Ltd., Osaka, Japan) at 100°C and allowed to mix for 2 h to obtain hydrophobically modified PLL (Scheme 1a). Subsequently, SA was added in 35-65 % molar ratios ($COOH/NH_2$) and was allowed to react for 2 h at 50 °C (Scheme 1b).

2.2 Characterization of polyampholytes

^{1}H NMR spectra were obtained at 25°C on a Bruker AVANCE III 400 spectrometer (Bruker BioSpin Inc., Switzerland) in D_2O.

2.3 Determination of critical aggregation concentration (CAC)

The critical aggregation concentrations (CACs) of the self-assemblies were investigated by measuring the excitation spectra of pyrene in polyampholyte solutions. The polyampholyte was dissolved in phosphate buffered saline without calcium and magnesium (PBS(-)) at different concentrations (0.01, 0.02, 0.05, 0.1, 0.2, 0.5, 1, 2, 5, and 10 mg/mL). Next, 4 μL of pyrene (1.0 mM in acetone) was transferred to a 10 mL test tube and acetone was completely volatilized under a gentle steam of nitrogen. Different concentrations of polyampholyte were added (4 mL) to each tube. The resulting solutions were sonicated in an ultrasonic bath for 30 min, then heated for 3 h at 65 °C to equilibrate the pyrene and the polyampholytes. Subsequently, the samples were left to cool overnight at room temperature. The emission spectra of pyrene were recorded from 300 to 360 nm on a JASCO FP-6500. The excitation/emission slits widths were set as 3/3 mm. Spectra were accumulated with a scan speed of 100 nm/min. The intensity of pyrene at 338 nm (I_{338}) and 335 nm (I_{335}) was plotted against the concentration of polyampholyte.

2.4 Particle size and zeta potential measurements

The mean hydrodynamic diameters and zeta potentials of the aggregated polyampholyte nanoparticles were determined by dynamic light scattering (DLS) method on a Zetasizer 3000 (Malvern Instruments, Worcestershire, UK) with a scattering angle of 135°. Polyampholytes were diluted with PBS(-) at 10 mg/mL and were used for measurements.

2.5 Morphological analysis

The morphology of the polyampholyte nanoparticles was detected using a Hitachi H-600 transmission electron microscope (TEM) operated at an accelerating voltage of 100 kV. A

drop of the polyampholyte nanoparticles was placed on a copper grid (200 mesh covered with carbon) and allowed to dry for 10 min prior to the measurement.

2.6 Preparation of protein-loaded polyampholyte nanoparticles and determination of protein adsorption on/into nanoparticles

To prepare the protein-loaded polyampholyte nanoparticles, bovine serum albumin (BSA) (Wako) and lysozyme (Wako) were chosen as model proteins. Polyampholyte nanoparticles (10 mg/mL) were mixed with the protein solutions (0.25, 0.5, 1.0, 2.0 mg/mL) of an equal volume, and were incubated for 2 h at room temperature and then centrifuged for 5 min at 10000 rpm using a centrifugal filter off (cut-off: 100 kDa for BSA and 50 kDa for lysozyme) in order to separate adsorbed and un-adsorbed proteins [31]. The amount of un-adsorbed protein was quantified by the Bradford assay using Bradford Ultra reagent (Expedeon Ltd., Harston, UK) at 595 nm. The adsorption efficacy was calculated using **Equation 3**.

Adsorption efficacy=(amount of protein adsorption/initial feeding amount of protein)*100 (**3**)

2.7 Cell culture

L929 cells (American Type Culture Collection, Manassas, VA, USA) were cultured in Dulbecco's modified Eagle's medium (DMEM; Sigma-Aldrich, St. Louis, MO) supplemented with 10% fetal bovine serum (FBS) at 37 ^{o}C under 5 % CO_2 in a humidified atmosphere. When the cells reached 80 % confluence, they were removed by 0.25 % (w/v) trypsin containing 0.02 % (w/v) ethylenediamine tetraacetic acid (EDTA) in PBS(-) and were seeded on a new tissue culture plate for subculture.

2.8 Cytotoxicity assay

Cells suspended in 0.1 mL medium at a concentration of 1.0 x 10^4 mL were placed in 96-well culture plates. After 72 h incubation at 37 °C, 0.1 mL medium containing different concentrations polyampholytes was added to the cells, followed by 48 h incubation. To evaluate cell viability, 0.1 mL 3-(4,5-dimethyl thial-2-yl)-2, 5-diphenyltetrazalium bromide (MTT) solution (300 mg/mL in medium) was added to the cultured cells. The cells were then incubated for 4 h at 37°C. After incubating, the resulting color intensity was measured by a microplate reader (Versa max, Molecular Devices Co., CA, USA) at 540 nm, and was proportional to the number of viable cells. The cytotoxicity was represented as the concentration of the compound that caused a 50% reduction in MTT uptake by a treated cell culture compared with the untreated control culture (IC_{50}) [24].

2.9 Fluorescent labeling of polyampholytes and proteins

Hydrophobically modified polyampholytes and model proteins were labeled with a fluorescent dye for allow for observation with a confocal laser scanning microscope (CLSM). For polyampholytes labeling, a solution of PLL (25 w/w%) was treated with fluorescein isothiocynate (FITC-I, Dojindo, Kumamoto, Japan) at a 1/100 molar ratio for 24 h at room temperature. FITC-PLL was purified by dialysis (molecular weight cut off 3 KDa; Spectra/Por, Spectrum Laboratories, Inc., CA, USA) against water for 3 days. The same procedure was used to obtain hydrophobically modified polyampholytes. For BSA and lysozyme labeling, Texas Red (TR) conjugation was carried out as described in Section 4.10.

2.10 TR labeling of proteins (lysozyme/BSA*)*

Lysozyme or BSA (2 mg) was dissolved in chilled buffer (sodium bicarbonate, 0.1 M) and 50 μL of TR sulfonyl chloride solution (Dojindo, 1 mg in 50 μL in acetonitrile) was added with rapid mixing. After incubating for 1 h, the reaction mixture was desalted using a desalting column (for BSA; 30K, lysozyme; 3K) which was equilibrated by PBS buffer.

2.11 Confirmation of freezing concentration

4.11.1 Solid state ^{1}H-NMR for determination of residual water

In order to measure the residual water during freezing, solid-state NMR experiments were performed on a 700-MHz JEOL ECA spectrometer, using a Doty Scientific Inc. (DSI) 4 mm HXY CP/MAS NMR probe. A DMSO saline solution (10 w/v%) and a saline solution of 7.5 % PLL-SA(65) were measured. The cryopreservation solution samples were sealed into DSI inner-sealing cells for an XC4 rotor and spun at 3.6-5.8 kHz at various temperatures ranging from 1 to -41 ^{o}C. The samples were cooled by replacing spinning and bearing gases with cooled N_2-gas passed through a liquid nitrogen cryostat with a DSI cold gas supply unit. All data were processed with the program NMRPipe [32]. NMRViewJ [33] was employed for spectral visualization and analysis. The intensities and line widths of the peaks were analyzed by IGOR (WaveMetrics). The contribution from frozen components was eliminated by baseline correction and line-shape analysis. The amount of residual water in ice was estimated by the peak intensities of the H_2O signal.

4.11.2. Cryomicroscopic observation of cells during freezing

The cryomicroscopy experimental procedures utilized here were similar to those described extensively in the literature [34,35]. We observed the L929 cells during freezing in the

cryopreservation solution (10% DMSO and 10% PLL-SA(65)) using the cryomicroscope. A small drop (4 μL) of the cell suspension was pipetted in the center of a quartz crucible (15 mm in diameter), covered, loaded on a cooling stage (Linkam 10002L Cooling Stage, Linkam Scientific Instruments, UK), and cooled to -80 ^{o}C at 1^{o}C/min. Ice was seeded at -2^{o}C using a needle, pre-cooled in liquid nitrogen to avoid supercooling. The morphology of the ice crystals was captured with a mounted photomicroscope (Digital Microscope, VHX-500, Keyence Corp., Tokyo, Japan).

2.12 Cell freezing with protein-loaded nanoparticles

To prepare protein-encapsulating polyampholyte nanoparticles, FITC-labeled polyampholyte nanoparticles (10mg/mL) and the same volume of TR-labeled protein (2mg/mL) were incubated for 2 h and centrifuged at 13200 g for 15 min. Un-adsorbed and adsorbed proteins were separated and washed by PBS(-) repeatedly.

L929 cells were counted and re-suspended in 1 mL of 10% polyampholyte (PLL-SA(65)) cryoprotective solution or 10% DMSO culture medium solution with protein-loaded polyampholyte nanoparticles (10 mg) without FBS at 4 ^{o}C at a density of 1x10^{6} cells/mL in 1.9 mL cryovials (Nalgene, Rochester, NY) and were stored in a -80 ^{o}C freezer overnight. These vials were thawed at 37°C, diluted with DMEM medium and cells were washed 3 times with DMEM. All cells were counted using a haemocytometer and the tryptan blue staining method. The reported viability values are the ratios of living cells to total cells. The adsorption of polyampholyte and encapsulated proteins onto L929 cells before and after freezing was observed using a CLSM (FV1000-D; Olympus, Tokyo, Japan).

2.13 Intracellular uptake of protein via endocytosis

After thawing, cells were again seeded in a glass bottom dish with DMEM and incubated for 3 days. Then they were washed with PBS(-) 3 times and were observed by a CLSM.

2.14 Statistical analysis

All data are expressed as the mean standard deviation (SD). Measurements for post-thaw viability were collected with n=5. All experiments were conducted in triplicate. Data among the different groups were compared using a one-way analysis of variance (ANOVA) with a post-hoc Tukey–Kramer test.

3. Results and Discussion

3.1 Synthesis of hydrophobic polyampholytes

In order to develop nanocarriers to load proteins, hydrophobically modified polyampholytes were synthesized by the reaction of DDSA and SA (Scheme 1) into PLL and were characterized by ^{1}H-NMR in D_2O. The degree of substitution of DDSA and SA was obtained by ^{1}H-NMR using Equation (1) and (2):

$$\text{Degree of substitution for DDSA (\%)} = (2*A_{\delta 0.74}/3*\ A_{\delta 1.5\text{-}1.8})*100 \quad (\mathbf{1})$$

$$\text{Degree of substitution for SA (\%)} = (2*A_{\delta 2.4}/4*\ A_{\delta 1.5\text{-}1.8})*100 \quad (\mathbf{2})$$

$A_{\delta 0.74}$ is the integral of the methyl peak from DDSA located at 0.74 ppm and $A_{\delta 2.4}$ is the integral of the methylene peak of SA located at 2.4 ppm. $A_{\delta 1.5\text{-}1.8}$ is the integral of the b-methylene peak of poly-lysine main chain located at from 1.5ppm (intact PLL) to 1.8ppm. The introduction rate of DDSA and SA was well controlled and is listed in Table 1. The ^{1}H-NMR spectra are shown in Fig.S1. In this study, we denoted the modified PLL as PLL-

DDSA(n)-SA (m), where *n* and *m* indicate the substitution value of DDSA and SA against the molar ratio of the amino groups, respectively. For example, PLL-DDSA(3)-SA(65) indicates that 3% of the amino groups have been substituted with DDSA and 65% of the amino groups have been substituted with SA, and PLL-SA(65) indicates that 65% of the amino groups have been substituted by SA without addition of DDSA. According to Huang et al., [36] PLL hydrophobically modified with octenyl succinic anhydride self-assembled into micelles. The term 'micelles' in their report indicated self-assembled polycore particles. Generally, the term 'polymer micelles' is used to represent self-assembled aggregates of amphiphilic block copolymers with a hydrophobic core and hydrophilic shell [37]. However, when modifications were carried out using DDSA or octenyl succinic anhydride, the hydrophobic moieties must have been introduced randomly in PLL. Therefore, the self-assembled aggregates should have had a hydrophobic poly-core as the cross-linking point, similar to nanogels [38]. As such, we describe the aggregation of hydrophobically modified PLL as nanoparticles in this study.

3.2 Characterization of polyampholyte nanoparticles

3.2.1 Nanoparticle size and morphology measurements

The size of nanoparticles has a strong influence in nanomedicines and can affect drug loading, drug release, and the stability of nanoparticles [39]. In terms of nanoparticle internalization into cells by endocytosis to achieve targeted delivery, an increase in particle size will decrease the uptake and affect the bioavailability and efficacy of drugs. Polyampholyte nanoparticles (10 mg/mL) were formulated by adding PBS(-). DLS

measurements revealed that that PLL-DDSA(3)-SA(35), PLL-DDSA(5)-SA(35), PLL-DDSA(3)-SA(65), and PLL-DDSA(5)-SA(65) had average sizes of 16.2, 15.7, 18.4, and 13.5 nm, respectively, with narrow size distributions (PDI 0.1-0.2) (Fig. 1a, Table 1). The DLS measurements correlated with TEM observations (Fig.1b), in that the hydrodynamic radius measured by DLS was almost equal to the size of the polyampholytes nanoparticles seen via TEM. Increased substitution of DDSA and SA led to smaller particles (around 13 nm) due to the compact packing of the hydrophobic groups. Characterization of the polyampholyte nanoparticles is summarized in Table 1.

TEM was used to visualize polyampholyte nanoparticles that were fabricated in PBS(-) at 1w/w %. The morphology of the nanoparticles was spherical as seen by TEM (Fig. 1b), and the nanoparticles were smooth with nearly homogeneous structures. The size of the particles was smaller than those reported by Yu et al., [36] in which PLL was treated with octenyl succinic anhydride (diameter c.a. 100 nm). This was likely due to the fact that the present nanoparticles exhibited intermolecular hydrophobic and electrostatic interactions which led to a more compact aggregation as compared to polycationic nanoparticles.

3.2.2 Aggregation of polyampholyte nanoparticles

CAC of the polyampholytes suggested the formation of self-assembled aggregates. The CACs of the hydrophobically modified PLLs were determined using the pyrene fluorescence excitation spectra method at 25°C [40,41]. Specifically, the excitation spectra of pyrene in PLL-DDSA(3)-SA(65) and PLL-DDSA(5)-SA(65) in PBS(-) are shown in Fig. 2a,c. Based on the excitation spectra of pyrene and the red shift of the spectra, the ratio of the intensities

of 338 nm to 335 nm (I_{338}/I_{335}) versus the concentration of PLL-DDSA(3)-SA(65) and PLL-DDSA(5)-SA(65) were plotted (Fig. 2b,d). The intensity and spectra of other polyampholytes are shown in Fig. S2. The CAC value was estimated as the cross-point when extrapolating the ratio of I_{338}/I_{335} at low and high concentration regions and was found to be 0.5 mg/mL for PLL-DDSA(3)-SA(35) and PLL-DDSA(3)-SA(65). However, the value decreased for PLL-DDSA(5)-SA(35) and PLL-DDSA(5)-SA(65) to around 0.1 mg/mL (Table 1). These results can be explained by the fact that the more hydrophobic polyampholytes (PLL-DDSA(5)-SA(35), or -(65)) had increased intermolecular interactions, which led to aggregate formation at a lower concentration.

3.2.3 Surface charges of nanoparticles

Zeta potential is an important characteristic for drug delivery. Surface charges can be governed by hydrophobicity and can influence particle stability [42]. To investigate the distribution of carboxyl groups on the surface, nanoparticles were suspended in PBS and the zeta potential was determined. The zeta potential of all polyampholytes was greatly affected by the balance between the amount of carboxyl groups and amino groups. Their surface charges were manipulated by the feed ratio of DDSA and SA. The zeta potentials of PLL-DDSA(3)-SA(35), PLL-DDSA(5)-SA(35), PLL-DDSA(3)-SA(65), and PLL-DDSA(5)-SA(65) were +4.08, +2.61, −13.1, and -14.0 mV, respectively (Table 1). The zeta potential of hydrophobically modified PLL decreased with increased substitution of SA, and the change was due to the carboxyl groups of SA near the surface. Moreover, it was confirmed that PLL-DDSA(3 and 5)-SA(35) were cationic nanoparticles and PLL-DDSA(3 and 5)-SA(65) were

anionic nanoparticles. On the other hand, PLL-SA(65) did not aggregate or have a zeta potential. As a comparison, it was previously reported that polyampholytes derived from poly(amino acids) without any hydrophobic modifications aggregated and showed negative and positive zeta potentials [31]. However, those polyampholytes had a molecular weight of more than 700000 and exhibited significant aggregation, whereas the current polyampholytes have a molecular weight of around 5000. The difference in molecular weight might explain why the nanoparticles required modification with hydrophobic moieties to induce aggregation.

3.3 Adsorption of proteins on/into polyampholyte nanoparticles

In order to evaluate protein adsorption on/into polyampholyte nanoparticles, we selected BSA (anionic protein) and lysozyme (cationic protein) as model proteins. The adsorption efficiency of lysozyme was greater with anionic nanoparticles (PLL-DDSA(5)-SA(65)), whereas the adsorption efficiency of BSA was more effective with cationic nanoparticles (Fig. 3a,c). This was ascribed to the strong electrostatic interactions between the hydrophobically modified nanoparticles and the proteins. The adsorption efficiency of BSA was almost 100% at 2 mg/mL, whereas lysozyme showed a 90% efficiency (Fig. 3b,d). These results revealed that we successfully developed two types of protein-loaded nanoparticles by electrostatic interactions.

3.4 Characterization of protein-loaded polyampholyte nanoparticles

2.4.1 Particle size of protein-loaded polyampholyte nanoparticles

The particle size of the protein-loaded nanoparticles (20 nm) was slightly larger than the bare nanoparticles. The particles sizes increased due to the strong electrostatic interactions between the nanoparticles and proteins, as shown in Fig. S3 and Table 2.

2.4.2 Stability of protein-loaded polyampholyte nanoparticles

We measured the average size of bare and protein-loaded polyampholyte nanoparticles stored at 25˚C for 7 d. The stability of polyampholyte nanoparticles was mainly affected by the particle size and distribution. Specifically, the size of bare polyampholyte nanoparticles did not change after incubation for 7 d in PBS(-), highlighting the stability of the nanoparticles (Fig. 4a). However, the size of the BSA-loaded PLL-DDSA(3 or 5)-SA(35) increased up to 3-fold during storage(Fig. 4b). In contrast, lysozyme-loaded PLL-DDSA(3 or 5)-SA(65) did not change in size. Notably, the zeta potential of PLL-DDSA(3 or 5)-SA(35) was a smaller absolute value than that of PLL-DDSA(3 or 5)-SA(65), and PLL-DDSA(3 or 5)-SA(35) nanoparticles aggregated.

3.5 Freeze concentration

When cells are frozen with the appropriate concentration of cryoprotectant, ice crystal formation excludes solutes and the remaining solution can be concentrated. The cells located in the residual solution are exposed to a high osmotic pressure, leading to dehydration. By avoiding intracellular ice formation, cells can survive freezing [43-45]. Cryomicroscopic observations revealed that after ice crystal formation, residual water can exist in the cryoprotectant solutions and cells are located in the residual concentrated solution (Fig. 5a).

The residual water ratio during freezing in the presence of two types of cryoprotectants, 10% DMSO and 10% PLL-SA(65), was determined by solid-state ^{1}H-NMR and is given in Fig. 5b. The cells were in the highly concentrated residual water during freezing. Kataoka et al. reported that this freeze concentration mechanism was useful in a click chemistry reaction by the condensation of the reactants [46]. We also expected that the proteins in the medium were concentrated around the cell membranes, and could enhance the adsorption of the concentrated proteins.

3.6 Enhancement of protein adsorption by freeze concentration

3.6.1 Cell viability after freezing

L929 cells were frozen with protein-loaded polyampholyte nanoparticles (2 mg protein and 1 w/w% nanoparticles in the cell suspension) with 10 % PLL-SA(65) as a cryoprotectant. The cell viability after freeze-thawing is given in Fig. 6. Over 80 % of cells survived freezing with 10 % DMSO and with 10 % PLL-SA(65). This result agreed with previous reports [24,47,48]. However, the cell viability after freezing with protein-loaded polyampholyte nanoparticles tended to decrease even with the addition of 10 % PLL-SA(65) as a cryoprotectant. Specifically, a significant decrease in the cell viability with PLL-DDSA(3 or 5)-SA(35) was observed. PLL-DDSA(5)-SA(65) showed less of a decrease, regardless of the nature of the cryoprotectant (i.e., 10 % DMSO or PLL-SA(65)). These results might be explained by the cytotoxicity of the nanoparticles. The viability with various concentrations of nanoparticles was plotted (Fig. S4) and the IC_{50} was 0.8 % (PLL-DDSA(3)-SA(35)), 1.0 % (PLL-DDSA(5)-SA(35)), 2.0 %(PLL-DDSA(3)-SA(65)), and 2.6 % (PLL-DDSA(5)-SA(65)). The

high cytotoxicity of PLL-DDSA(3 or 5)-SA(35) may be due to the positive zeta-potential of the nanoparticles. The viability of cells with the positively charged nanoparticles was 60 %, whereas it was 80 % with the negatively charged nanoparticles. Therefore, we chose PLL-DDSA(3 or 5)-SA(65) for use in protein delivery by freeze concentration, as described in the following section.

3.6.2 Cellular delivery and uptake of BSA/Lysozyme delivered by the nanoparticles

Fig. 7a,b,c show the confocal microscope images of L929 cells before and after freezing in the presence of TR-conjugated, protein-loaded FITC-conjugated polyampholyte nanoparticles with 10% PLL-SA(65) as a cryoprotectant. When cell were frozen in the presence of the FITC-conjugated PLL-SA(65) (TR-conjugated lysozyme), almost no fluorescence was observed around the cell membrane (Fig. 7a). Without DDSA, PLL-SA(65) did not form stable nanoparticles (Table 1) and showed no aggregation with lysozyme. Even if freeze concentration occurred, the concentrated polyampholyte and lysozyme might have had a weak affinity towards the cell membrane after thawing, and the protein would have diffused into the thawed solution. However, a high florescence (both FITC and TR) was observed on the cells after thawing (Fig. 7b,c), clearly indicating that the protein-loaded nanoparticles were condensed on the peripheral cell membrane by freeze concentration because of the high affinity between the cell membrane and the hydrophobic moieties of the nanoparticles. When poly(vinyl alcohol) and poly(ethylene glycol) modified with hydrophobic alkyl chains were added to cells, the micelle-like nanoparticles easily adsorbed on the cell membrane [49]. In the present study, the concentrations of the nanoparticles and the proteins were too low to

identify the fluorescence on the cells, but the hydrophobicity of the polyampholyte nanoparticles was strong enough to facilitate absorption onto the cell membrane, preventing diffusion into the medium after thawing. The enhanced protein adsorption to cells by freeze concentration occurred not only when PLL-SA(65) was used as a cryoprotectant, but also when DMSO was used (Fig. S5). The fluorescence intensity with the two cryoprotectants was evaluated quantitatively using confocal microscopy. As shown in Fig. 8, the fluorescence of TR, which was normalized by the intensity of each unfrozen control (white bar =100%), was significantly higher than that of the unfrozen cells with PLL-DDSA(3)-SA(65) and PLL-DDSA(5)-SA(65). The intensity was higher when PLL-SA(65) was used as compared to when DMSO was used, possibly because of a higher freeze concentration (Fig. 5b). When the cells were frozen without cryoprotectants, cells did not survive and a very high fluorescence was observed because of cell membrane rupture (Fig. S6). In addition, when PLL-DDSA(3 or 5)-SA(35) was used as a nanocarrier for BSA, enhanced TR-conjugated BSA adsorption was observed (Fig. S7). However, the cytotoxicity of the cationic nanoparticles resulted in the low viability of the cells (viability 60%, Fig. 6).

3.6.3 Internalization of protein-loaded nanoparticles by endocytosis

To evaluate the endocytotic uptake of BSA- and lysozyme-loaded polyampholyte nanoparticles by L929 cells, cells were seeded and incubated after thawing. Confocal microscopic images of cells frozen in the presence of lysozyme and PLL-SA(65) and lysozyme-loaded PLL-DDSA(3 and 5)-SA(65) nanoparticles are given in Fig. 9. From the four photos of the upper row, weak FITC and TR fluorescence was observed for the cells

frozen without nanoparticles. In contrast, when cells were frozen with protein-loaded PLL-DDSA(3 and 5)-SA(65), a much higher fluorescence was obtained (middle and lower rows in Fig. 9). This clearly indicated that adsorbed protein and nanoparticles were internalized by endocytosis during culture. The mean intensity of the red fluorescence of cells is shown in Fig. 10. Each intensity was normalized by the intensity of the red fluorescence of the internalized TR-loaded lysozyme frozen without nanoparticles. This showed that a significantly higher internalization occurred when proteins were loaded with hydrophobically modified polyampholyte nanoparticles. The higher hydrophobicity enhanced the endocytosis of the protein-loaded nanoparticles. This result agreed the results of a previous study which showed that hydrophobic nanoparticles were easily internalized into cells by endocytosis [50,51]. When BSA-loaded PLL-DDSA(3 and 5)-SA(35) were used, similar results were obtained (Fig. S8).

4. Conclusions

Here we demonstrated the successful, efficacious, and safe delivery of proteins to cells using freeze concentration. First, we developed self-assembled hydrophobic polyampholyte nanoparticles as delivery vehicles. These nanoparticles had narrow size distributions, exhibited positive and negative surface charges, and were used to adsorb and encapsulate model proteins lysozyme and BSA. Confocal fluorescence micrographs revealed that nanoparticles delivered their contents efficiently into the cytosol of cells after freezing. These results provided encouraging evidence for the development of an effective method for the cytoplasmic introduction of proteins. This technique might be useful for antigen cytoplasmic

delivery to immune cells for immunotherapy or for gene delivery for gene therapy. In conclusion, freezing appeared to be a promising and versatile system for enhanced adsorption and internalization of drugs in vitro. Although further optimization of the cytotoxicity and protein adsorption onto the carriers should be conducted, we expect that this methodology can be globally applicable for the facile enhancement of protein delivery with nanocarriers.

Acknowledgements
This study was supported in part by a Grant-in-Aid, KAKENHI (25870267) for Scientific Research from the Ministry of Education, Culture, Sports, Science and Technology, Japan.

Disclosures
The authors have no conflicts of interest to declare.

References

[1] Sengupta S, Eavarone D, Capila I, Zhao G, Watson N, Kiziltepe T, et al. Temporal targeting of tumour cells and neovasculature with a nanoscale delivery system. Nature 2005;436:568-572.

[2] Lundy BB, Convertine A, Miteva M, Stayton PS. Neutral polymeric micelles for RNA delivery. Bioconjug Chem 2013;24:398-407.

[3] Deng C, Jiang Y, Cheng R, Meng F, Zhong Z. Biodegradable polymeric micelles for targeted and controlled anticancer drug delivery: Promises, progress and prospects. Nano Today 2012;7:467-480.

[4] Nishiyama N, Kataoka K. Current state, achievements, and future prospects of polymeric micelles as nanocarriers for drug and gene delivery. Pharmacol Ther 2006;112:630–648.

[5] Sakaguchi N, Kojima C, Harada A, Kono K. Preparation of pH-Sensitive poly(glycidol) derivatives with varying hydrophobicities: Their ability to sensitize stable liposomes to pH. Bioconjug Chem 2008;19:1040-1048.

[6] Han S, Mahato RI, Kim SW. Water-soluble lipopolymer for gene delivery. Bioconjug Chem 2001;12:337-345.

[7] Takeuchi Y, Kurohane K, Ichikawa K, Yonezawa S, Ori H, Koishi T, et al. Polycation liposome enhances the endocytic uptake of photosensitizer into cells in the presence of serum. Bioconjug Chem 2003;14:790-796.

[8]Sahoo SK, Panda AK, Labhasetwae V, Characterisation of porous PLGA/PLA microparticles as scaffold for three dimensional growth of breast cancer cells. Biomacromolecules 2005;6:1132-1139.

[9] Kadir MA, Kim SJ, Ha EJ, Cho HY, Kim BS, Choi D, et al. Encapsulation of nanoparticles using nitrilotriacetic acid end-functionalized polystyrenes and their application for the separation of proteins. Adv Funct Mater 2012;22:4032-4037.

[10] Xie J, Li Y, Xu C, Xia M, Qin M, Wei J, et al. Photo synthesis of protein-based drug-delivery nanoparticles for active tumor targeting. Biomater Sci 2013;1:1216-1222.

[11] Li Y, Xiao K, Luo J, Lee J, Pan S, Lam KS. A novel size-tunable nanocarrier system for targeted anticancer drug delivery. J Control Release 2010;144:314–323.

[12] Takahashi H, Tahara Y, Sawada S, Akiyoshi K. Cationic amphiphilic polysaccharide nanoballs: protein stabilization and intracellular delivery by nano-encapsulation. Biomater Sci 2013;1:842-849.

[13] Maciel D, Figueira P, Xiao S, Hu D, Shi X, Rodrigues J, et al. Redox-responsive alginate nanogels with enhanced anticancer cytotoxicity. Biomacromolecules 2013;14:3140-3146.

[14] Larson N, Ghandehari H. Polymeric conjugates for drug delivery. Chem Mater 2012;24:840-853.

[15] Wu X, Song Y, Han J, Yang L, Han S. Traceless protein delivery with an efficient recyclable nanocarrier. Biomater Sci 2013;1:918-923.

[16] Salmaso S, Bersani S, Mastrotto F, Tonon G, Schrepfer R, Stefano G, et al. Self-assembling nanocomposites for protein delivery: Supramolecular interactions between PEG-cholane and rh-G-CSF. J Control Release 2012;162:176-184.

[17] Serwer LP, James CD. Challenges in drug delivery to tumors of the central nervous system: An overview of pharmacological and surgical considerations. Adv Drug Deliv Rev 2012;64:590-597.

[18] Vasir JK, Labhasetwar V. Biodegradable nanoparticles for cytosolic delivery of therapeutics, Adv Drug Deliv Rev 2007;59:718-728.

[19] Yamashita F, Hashida M. Pharmacokinetic considerations for targeted drug delivery; Adv Drug Deliv Rev 2013;65:139-147.

[20] Benoit D, Boutin M, Controlling mesenchymal stem cell gene expression using polymer mediated delivery of siRNA. Biomacromolecules 2012;13:3841-3849.

[21] Cheng R, Feng F, Meng F, Deng C, Feijen J, Zhong Z. Glutathione-responsive nano-vehicles as a promising platform for targeted intracellular drug and gene delivery. J Control Release 2011;152:2-12.

[22] P. Englezos. The freeze concentration process and its applications. Dev Chem Eng Mineral Process 1994;2:3-15.

[23] Pham QT. Advances in food freezing/thawing/freeze concentration modelling and techniques. Jpn J Food Eng 2008;9:21-32.

[24] Matsumura K, Hyon SH. Polyampholytes as low toxic efficient cryoprotective agents with antifreeze protein properties. Biomaterials 2009;30:4842-4849.

[25] Matsumura K, Bae JY, Kim HH, Hyon SH. Effective vitrification of human induced pluripotent stem cells using carboxylated e-poly-L-lysine. Cryobiology 2011; 63:76-83.

[26] Rajan R, Jain M, Matsumura K. Cryoprotective properties of completely synthetic polyampholytes via reversible addition-fragmentation chain transfer (RAFT) polymerization and the effects of hydrophobicity. J Biomater Sci Polym Ed 2013;24:1767-1780.

[27] Jain M, Rajan R, Hyon SH, Matsumura K. Hydrogelation of dextran-based polyampholytes with cryoprotective properties via click chemistry. Biomater Sci 2014;2:308-317.

[28] Yuba E, Harada A, Sakanishi Y, Watarai S, Kono K. A liposome-based antigen delivery system using pH-sensitive fusogenic polymers for cancer immunotherapy. Biomaterials 2013;34:3042-3052.

[29] Annette AR, Vandermeulen GWM, Klok HA. Advanced drug delivery devices via self-assembly of amphiphilic block copolymers. Adv Drug Deliv Rev 2001;53:95-108.

[30] Liu R, Lai Y, He B, Li Y, Wang G, Chang S, et al. Supramolecular nanoparticles generated by the self-assembly of polyrotaxanes for antitumor drug delivery Int J Nanomedicine 2012;7:5249-5258.

[31] Shen H, Akagi T, Akashi M. Polyampholyte nanoparticles prepared by self-complexation of cationized poly(g-glutamic acid) for protein carriers. Macromol Biosci 2012;12:1100-1105.

[32] Delaglio F, Grzesiek S, Vuister GW, Zhu G, Pfeifer L, Bax A. NMRPipe: a multidimensional spectral processing system based on UNIX pipes. J Biomol NMR 1995;6:277-293.

[33] Johnson BA. Using NMRView to visualize and analyze the NMR spectra of macromolecules. Methods Mol Biol 2004;278:313-352.

[34] Guha A, Devireddy R. Polyvinylpyrrolidone (PVP) mitigates the damaging effects of intracellular ice formation in adult stem cells. Ann Biomed Eng 2010;38:1826-1835.

[35] Balasubramanian SK, Bischof JC, Hubel A. Water transport and IIF parameters for a connective tissue equivalent. Cryobiology 2006;82:62-73.

[36] Yu H, Huang Y, Huang Q. Synthesis and characterization of novel antimicrobial emulsifiers from ε-polylysine. J Agric Food Chem 2010;58:1290-1295.

[37] Kataoka K, Matsumoto T, Yokoyama M, Okano T, Sakurai Y, Fukushima S. et al. Doxorubicin-loaded poly(ethylene glycol)–poly(β-benzyl-l-aspartate) copolymer micelles: their pharmaceutical characteristics and biological significance. J Control Release 2000;64:143-153.

[38] Akiyoshi K, Deguchi S, Moriguchi N, Yamaguchi S, Sunamoto J. Self-aggregates of hydrophobized polysaccharides in water. Formation and characteristics of nanoparticles. Macromolecules 1993;26:3062-3068.

[39] Balasubramanian SK, Poh KW, Ong CN, Kreyling WG, Ong WY, Yu LE. The effect of primary particle size on biodistribution of inhaled gold nano-agglomerates. Biomaterials 2013;34:5439-5452.

[40] Ananthapadmanabhan KP, Goddard ED, Turro NJ, Kuo PL. Fluorescence probes for critical micelle concentration determination. Langmuir 1985;1:352-355.

[41] Astafieva I, Zhong XF, Eisenberg A. Critical micellization phenomena in block polyelectrolyte solutions. Macromolecules 1993;26:7339-7352.

[42] Mora-Huertas CE, Fessi H, Elaissari A. Polymer-based nanocapsules for drug delivery. Int J Pharm 2010;385:113-142.

[43] Mazur P, Seki S, Pinn IL, Kleinhans FW, Edashige K. Extra- and intracellular ice formation in mouse oocytes. Cryobiology 2005;51:29–53.

[44] Matsumura K, Hayashi F, Nagashima T, Hyon SH. Cryoprotective properties of polyampholytes. Cryobiology and Cryotechnology 2013;59:23-28.

[45] Mandumpal JB, Kreck CA, Mancera RL. A molecular mechanism of solvent cryoprotection inaqueous DMSO solutions. Phys Chem Chem Phys 2011;13:3839–3842.

[46] Takemoto H, Miyata K, Ishii T, Hattori S, Osawa S, Nishiyama N, et al. Accelerated polymer−polymer click conjugation by freeze−thaw treatment. Bioconjug Chem 2012;23:1503-1506.

[47] Matsumura K, Bae JY, Hyon SH. Polyampholytes as cryoprotective agents for mammalian cell cryopreservation. Cell Transplant 2010;19:691–699.

[48] Matsumura K, Hayashi F, Nagashima T, Hyon SH. Long-term cryopreservation of human mesenchymal stem cells using carboxylated poly-L-lysine without the addition of proteins or dimethyl sulfoxide. J Biomater Sci Polym Ed 2013;24:1484-1497.

[49] Inui O, Teramura Y, Iwata H. Retention dynamics of amphiphilic polymers PEG-lipids and PVA-alkyl on the cell surface. ACS Appl Mater Interfaces 2010;2:1514–1520.

[50] Wu B, Tang S, Chen M, Zheng N. Amphiphilic modification and asymmetric silica encapsulation of hydrophobic Au–Fe3O4 dumbbell nanoparticles. Chem Commun 2014;50:174-176.

[51] Ding H, Ma Y. Interactions between Janus particles and membranes. Nanoscale 2012;4:1116-1122.

Scheme 1. Preparation of hydrophobically modified polyampholytes.

Figure 1. Size of polyampholyte nanoparticles prepared in PBS buffer (10 mg/mL). (a) Size distribution of different substituted polyampholyte nanoparticles as measured by DLS. (b) A typical TEM image of polyampholyte nanoparticles. The bars: 100 nm.

Figure 2. Determination of CACs of different nanoparticles. Pyrene excitation spectra of (a) PLL-DDSA(3)-SA(65) and (c) PLL-DDSA(5)-SA(65) solutions at different concentrations (A-J) 10, 5, 2, 1, 0.5, 0.2, 0.1, 0.05, 0.02, and 0.01 mg/mL, respectively. Plot of the ratio of I_{338}/I_{335} against the logarithm of the concentration of (b) PLL-DDSA(3)-SA(65) and (d) PLL-DDSA(5)-SA(65). The change in slope corresponded to the CAC of each polyampholyte.

Figure 3. Protein adsorption on/into nanoparticles. Amount of (a) BSA and (c) lysozyme adsorption on/into polyampholyte nanoparticles and their adsorption efficiency with different concentrations of (b) BSA and (d) lysozyme. Data are expressed as the mean ± SD. ***$P < 0.001$.

Figure 4. Size change of (a) bare and (b) protein-loaded polyampholyte nanoparticles versus the incubation time at 25^{o}C.

Figure 5. Freeze concentration during cell freezing with a cryoprotectant. (a) Cryomicrophotographs of cell suspension from -10 ^{o}C to -80 ^{o}C in the presence of 10 % DMSO. Cells were located in the remaining concentrated solution. The bar: 10μm. (b) Ratio of residual water during freezing with 10% DMSO and PLL-SA(65) measured by solid state ^{1}H-NMR.

Figure 6. Cell viability after being frozen at -80 ^{o}C for 1 d with various protein-loaded nanoparticles in the presence of 10% PLL-SA(65) as a cryoprotectant. Cells were also frozen with cryoprotective solutions (10% DMSO and 10% PLL-SA(65); left two columns) alone. Data are expressed as the mean ± SD. ***P < 0.001, **P<0.01.

Figure 7. Confocal microphotographs of L929 cells before and after freezing with various protein-loaded polyampholyte nanoparticles with 10% PLL-SA(0.65) as a cryoprotectant. (a) Cells were frozen with lysozyme (2mg) and PLL-SA(65). (b) Cell were frozen with protein-loaded PLL-DDSA(3)-SA(65) (lysozyme 2 mg, nanoparticles 10 mg in 1 mL DMEM). (c) Cells were frozen with protein-loaded PLL-DDSA(5)-SA(65) (lysozyme 2 mg, nanoparticles 10 mg in 1mL). Nanoparticles were stained with FITC and lysozyme was stained with TR. The bars: 10μm.

Figure 8. Quantitative analysis of fluorescence ratio of lysozyme adsorbed onto cells before and after being frozen with various protein-loaded nanoparticles. Data are expressed as the mean ± SD. ***P < 0.001.

Figure 9. Protein internalization via endocytosis during culture after being frozen with lysozyme and PLL-(SA) and lysozyme-loaded PLL-DDSA(3 or 5)-SA(65) nanoparticles with 10% PLL-SA(65) as a cryoprotectant. The bars: 10μm.

Figure 10. Quantitative analysis of fluorescence ratio of lysozyme internalized into cells after being frozen with various protein-loaded nanoparticles, against that with only PLL-SA(65). Data are expressed as the mean ± SD. ***P < 0.001.

Table 1. Summary of composition of polyampholyte nanoparticles including ^{1}H-NMR, diameter, polydispersity, zeta-potential, and CAC.

Samples	Composition in feed (molar %)		Composition in polymer (molar %)[a]		Diameter[b] (nm)	polydispersity[b]	Zeta potential[b] (mV)	CAC[c] (mg/mL)
	DDSA	SA	DDSA	SA				
PLL-SA(65)	0	65	0	63.5	ND	ND	ND	ND
PLL-DDSA(3)-SA(35)	3	35	2.7	34.8	16.15±0.23	0.165	+4.08	0.52
PLL-DDSA(5)-SA(35)	5	35	2.8	33.7	15.72±0.15	0.171	+2.61	0.14
PLL-DDSA(3)-SA(65)	3	65	4.8	64.2	18.56±0.44	0.167	-13.1	0.50
PLL-DDSA(5)-SA(65)	5	65	4.6	63.8	13.48±0.41	0.177	-14.0	0.11

a) Determined by ^{1}H-NMR, ND: Not detected.
b) Determined by DLS.
c) Determined using excitation spectra of pyrene.

Table 2. The size of hydrophobically modified polyampholyte nanoparticles before and after protein adsorption.

Samples	Diameter before protein adsorption (nm)	Diameter after protein adsorption (nm)
PLL-DDSA(3)-SA(35)	16.15±0.23	22.61±0.16
PLL-DDSA(5)-SA(35)	15.72±0.15	19.57±0.28
PLL-DDSA(3)-SA(65)	18.56±0.44	22.40±0.17
PLL-DDSA(5)-SA(65)	13.48±0.41	24.65±0.38

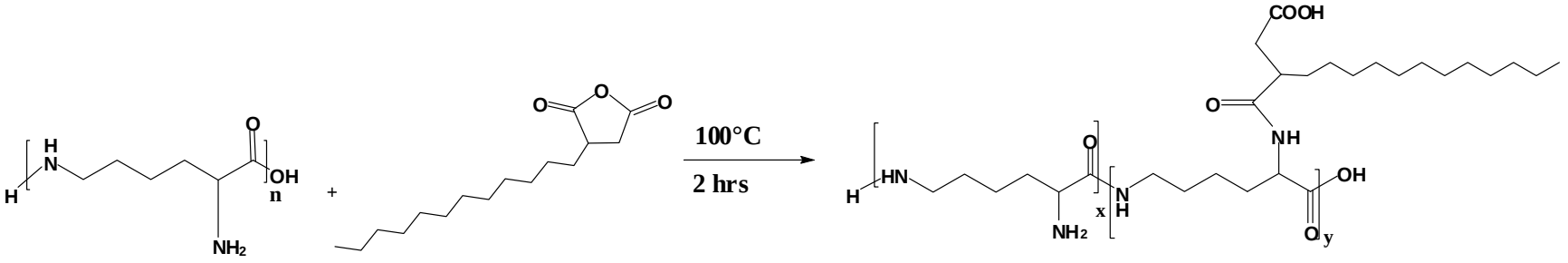

Epsilon Poly-l-lysine **Dodecylsuccinic anhydride** **PLL-DDSA**

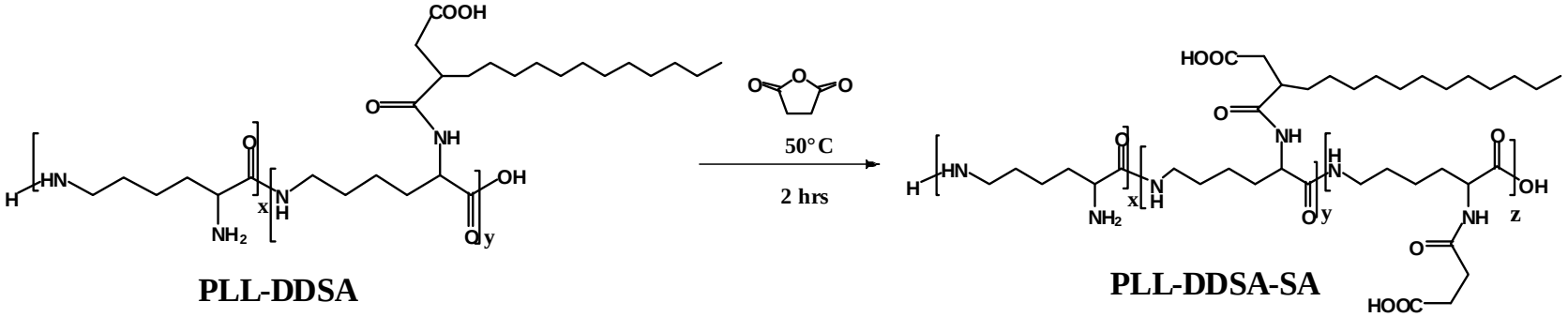

PLL-DDSA **PLL-DDSA-SA**

Scheme 1

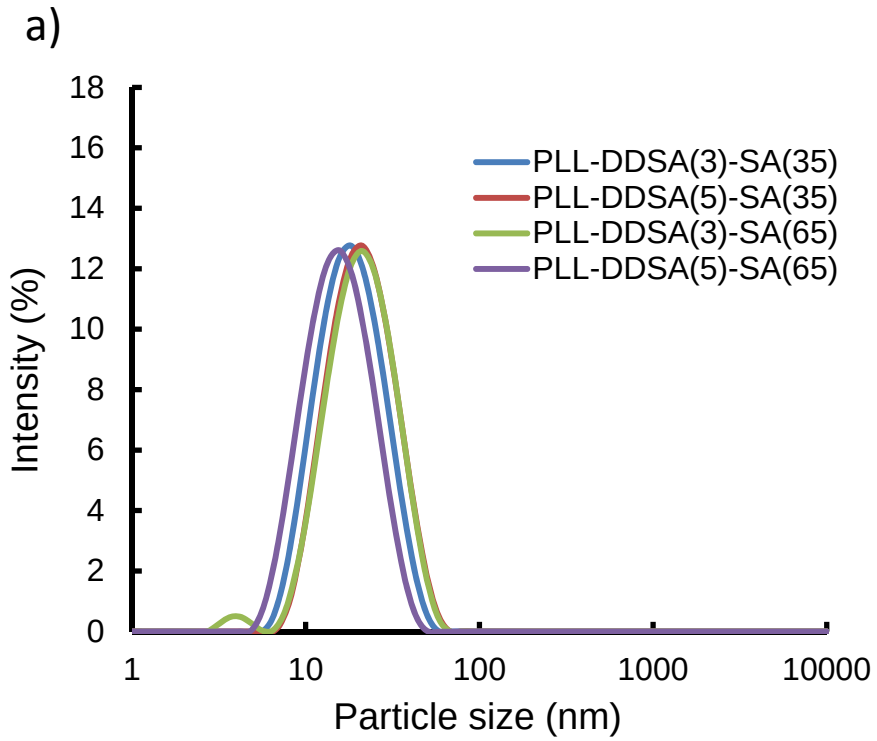
a)
18
16
14
12
10
8
6
4
2
0
Intensity (%)
1
10
100
1000
10000
Particle size (nm)
PLL-DDSA(3)-SA(35)
PLL-DDSA(5)-SA(35)
PLL-DDSA(3)-SA(65)
PLL-DDSA(5)-SA(65)

Fig.1A

b)

PLL-DDSA(3)-SA(35)

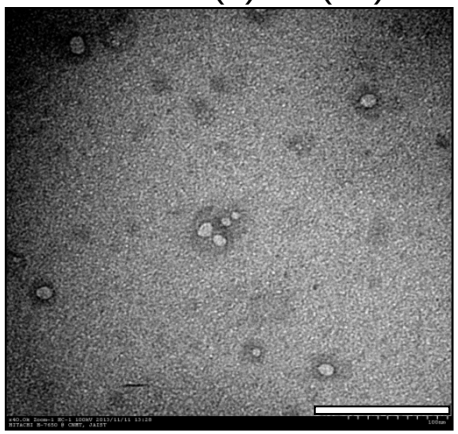

PLL-DDSA(5)-SA(35)

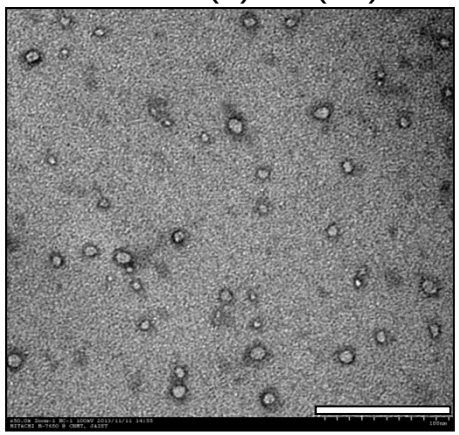

PLL-DDSA(3)-SA(65)

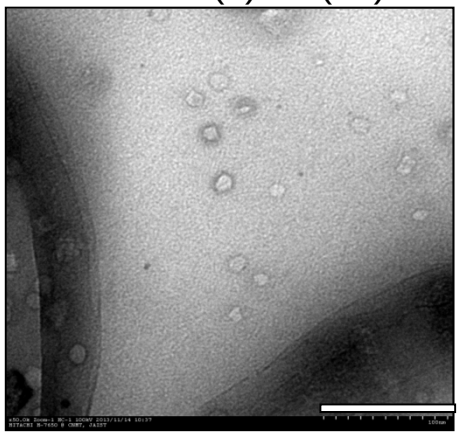

PLL-DDSA(5)-SA(65)

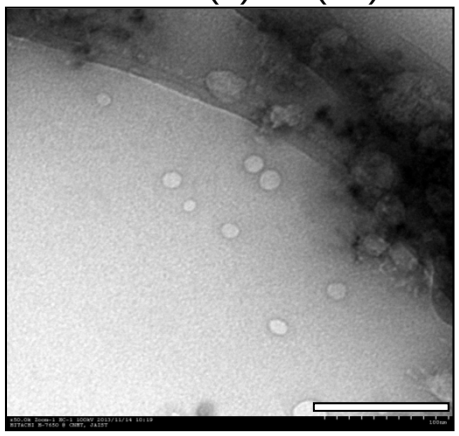

Fig.1B

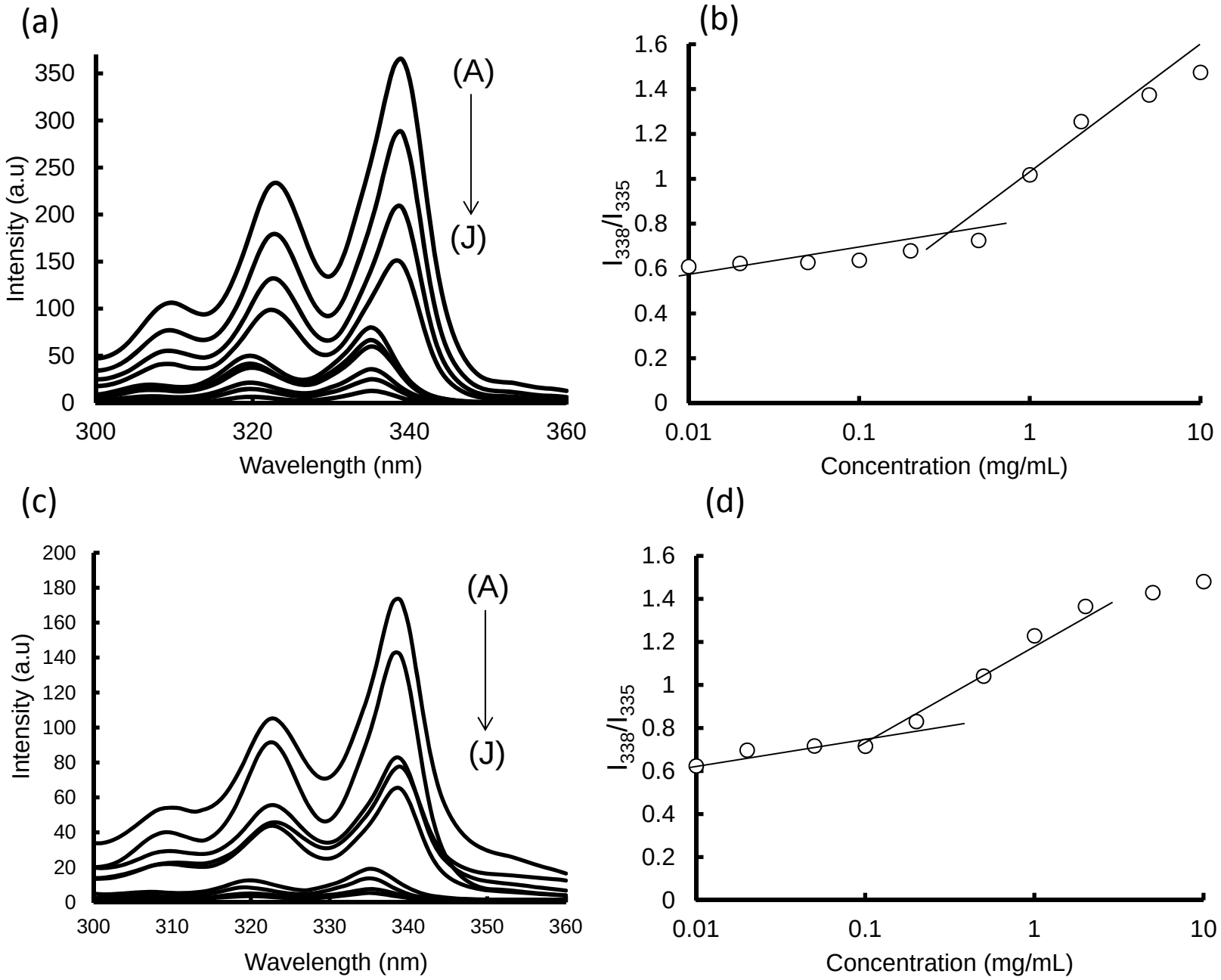
(a)
(A)
(J)
Intensity (a.u)
Wavelength (nm)
(b)
I_{338}/I_{335}
Concentration (mg/mL)
(c)
(A)
(J)
Intensity (a.u)
Wavelength (nm)
(d)
I_{338}/I_{335}
Concentration (mg/mL)

Fig.2

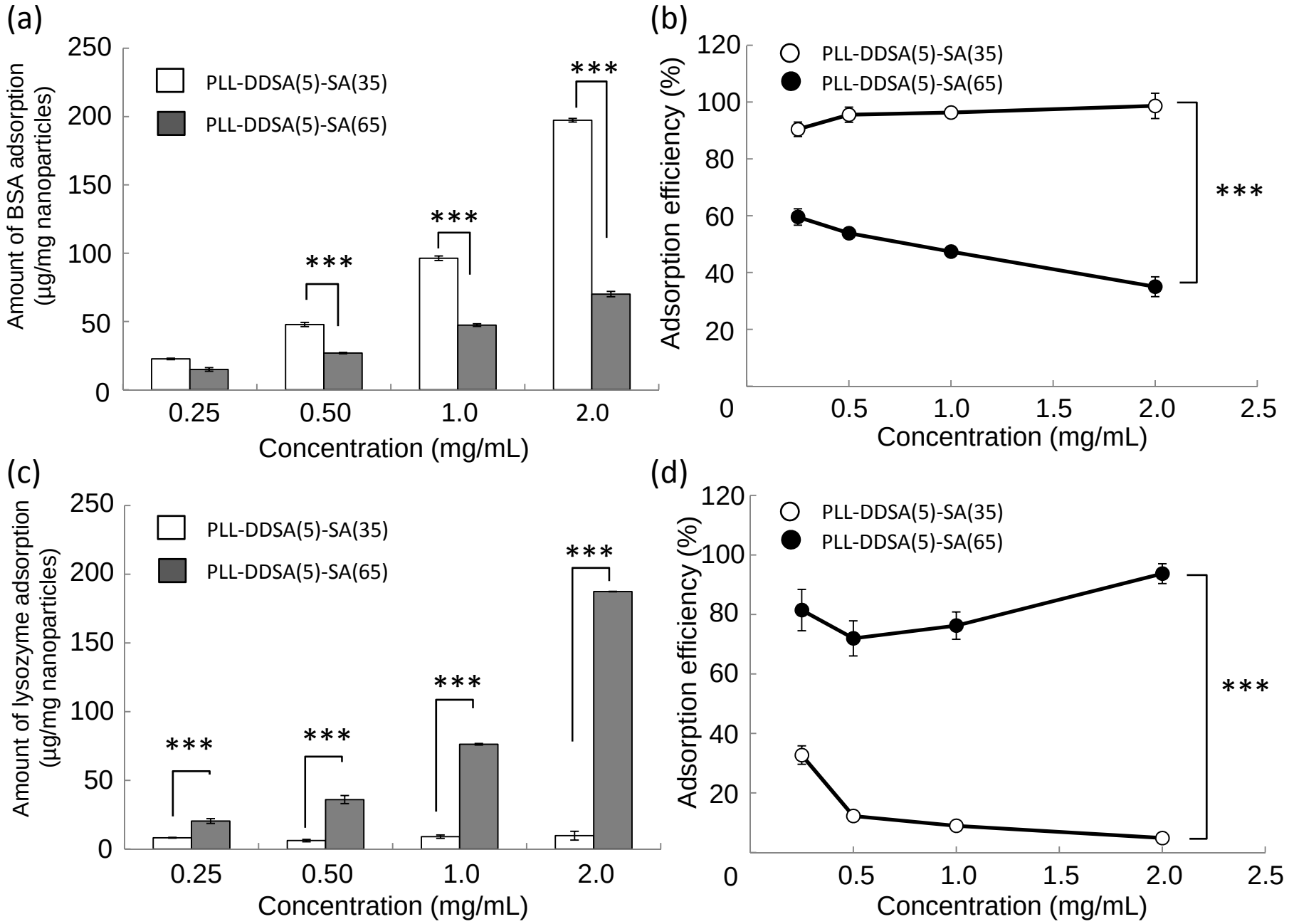
(a)
Amount of BSA adsorption (μg/mg nanoparticles)
PLL-DDSA(5)-SA(35)
PLL-DDSA(5)-SA(65)
***
Concentration (mg/mL)
(b)
Adsorption efficiency (%)
PLL-DDSA(5)-SA(35)
PLL-DDSA(5)-SA(65)
***
Concentration (mg/mL)
(c)
Amount of lysozyme adsorption (μg/mg nanoparticles)
PLL-DDSA(5)-SA(35)
PLL-DDSA(5)-SA(65)
***
Concentration (mg/mL)
(d)
Adsorption efficiency (%)
PLL-DDSA(5)-SA(35)
PLL-DDSA(5)-SA(65)
***
Concentration (mg/mL)

Fig.3

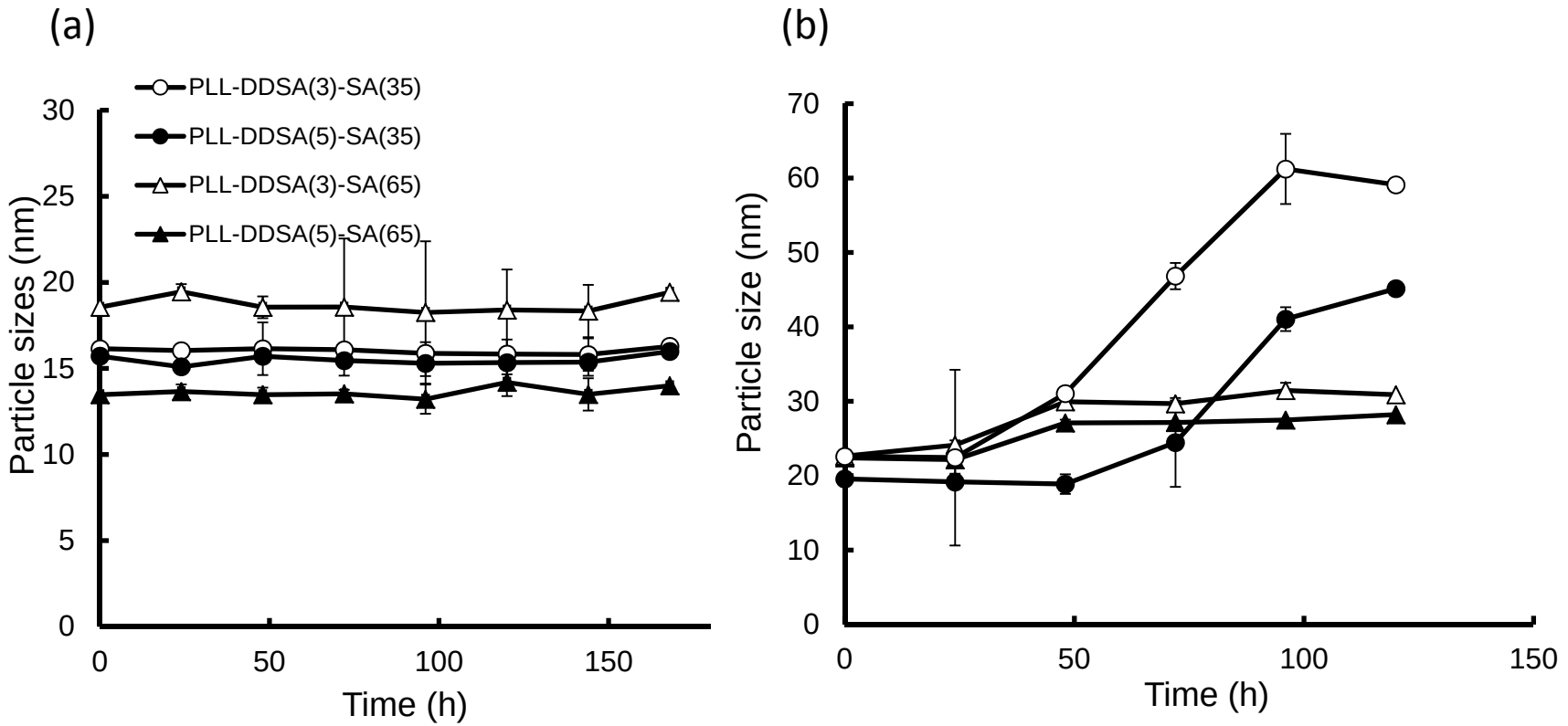
(a)
PLL-DDSA(3)-SA(35)
PLL-DDSA(5)-SA(35)
PLL-DDSA(3)-SA(65)
PLL-DDSA(5)-SA(65)
Particle sizes (nm)
Time (h)
(b)
Particle size (nm)
Time (h)

Fig. 4

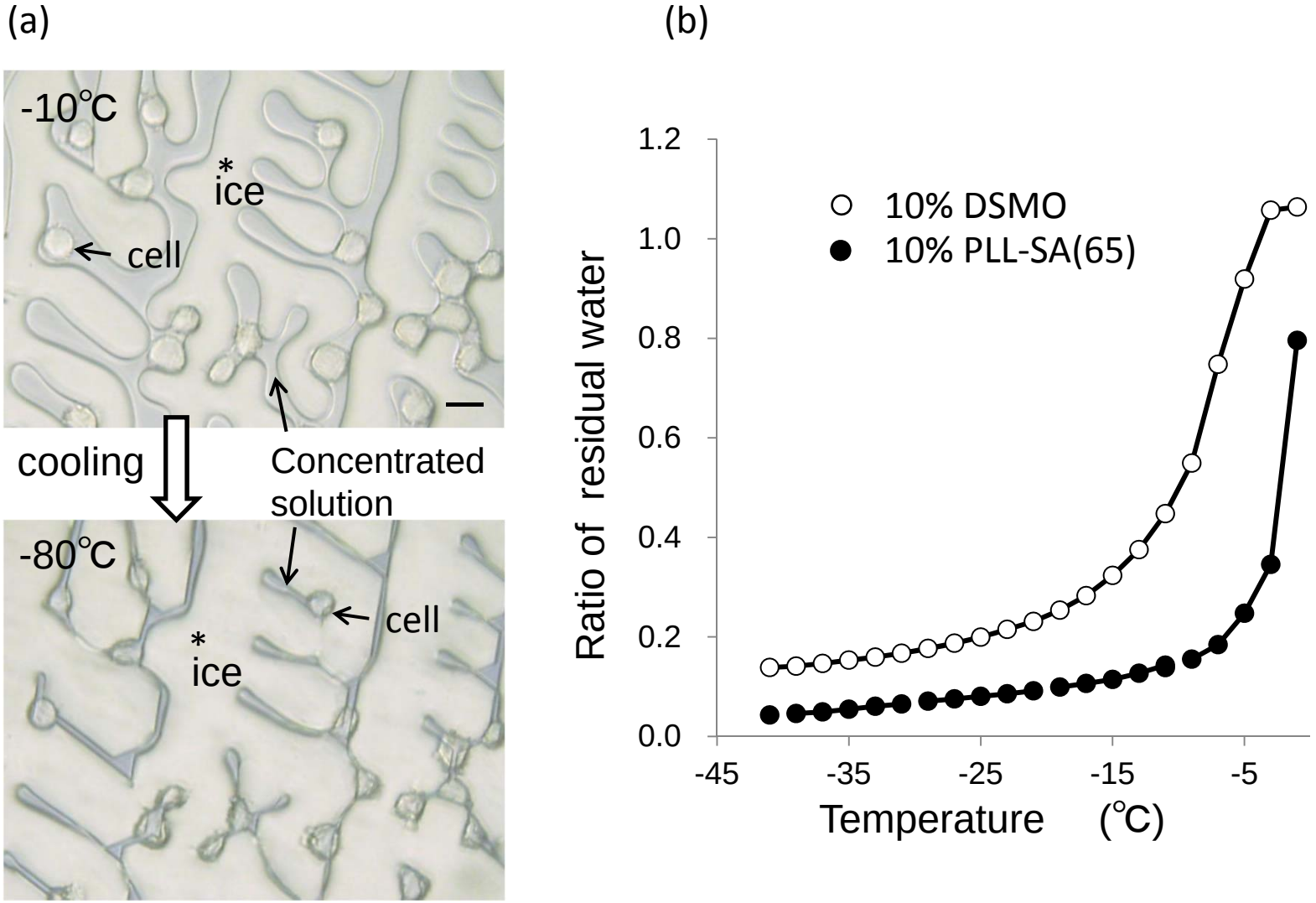
(a)
-10℃
ice
cell
cooling
Concentrated solution
-80℃
cell
ice
(b)
10% DSMO
10% PLL-SA(65)
Ratio of residual water
1.2
1.0
0.8
0.6
0.4
0.2
0.0
-45
-35
-25
-15
-5
Temperature (℃)

Fig.5

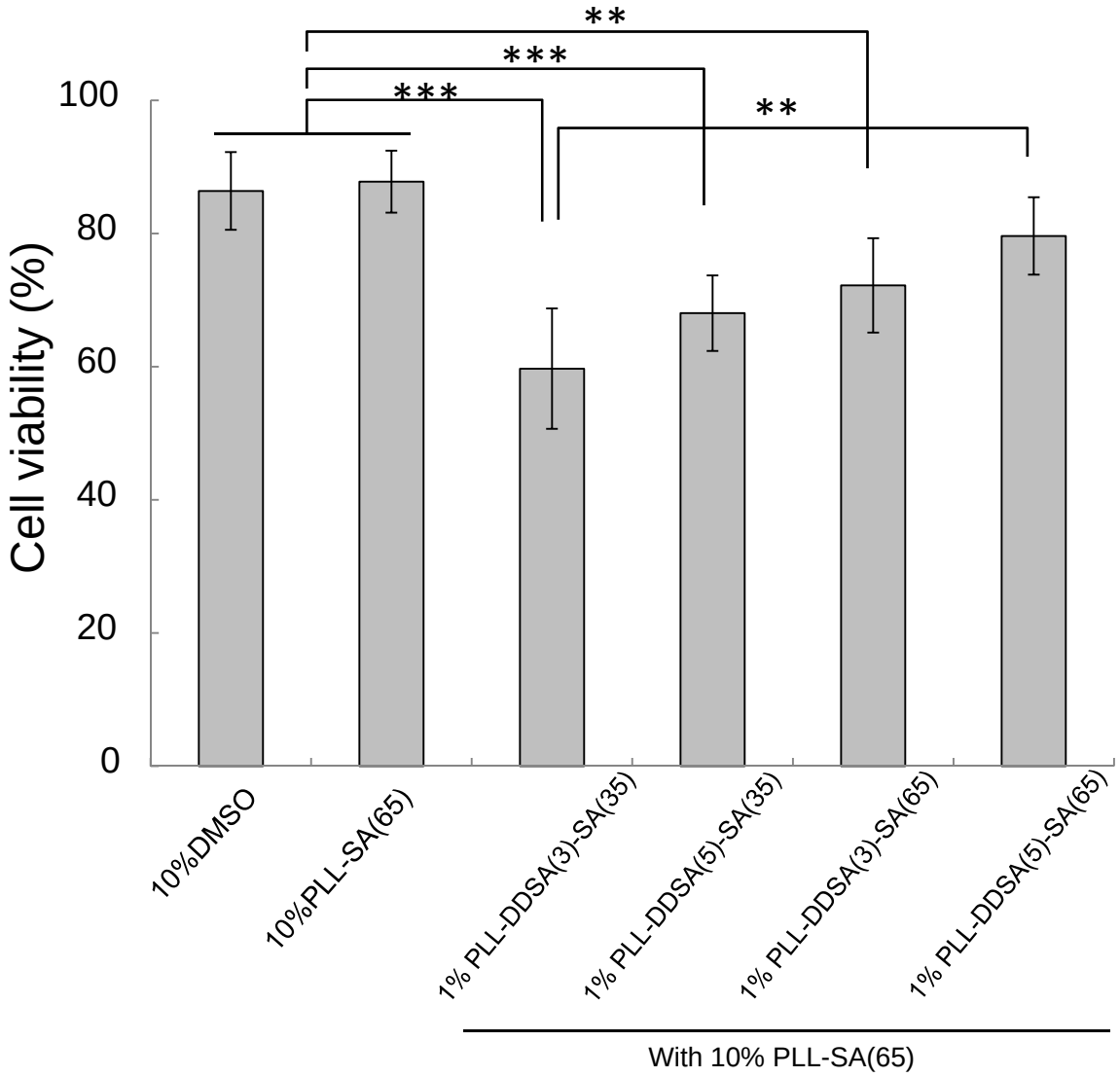
**
***
***
**
100
80
60
40
20
0
Cell viability (%)
10%DMSO
10%PLL-SA(65)
1% PLL-DDSA(3)-SA(35)
1% PLL-DDSA(5)-SA(35)
1% PLL-DDSA(3)-SA(65)
1% PLL-DDSA(5)-SA(65)
With 10% PLL-SA(65)

Fig.6

(a) Cells frozen with mixture of protein and PLL-SA(65)

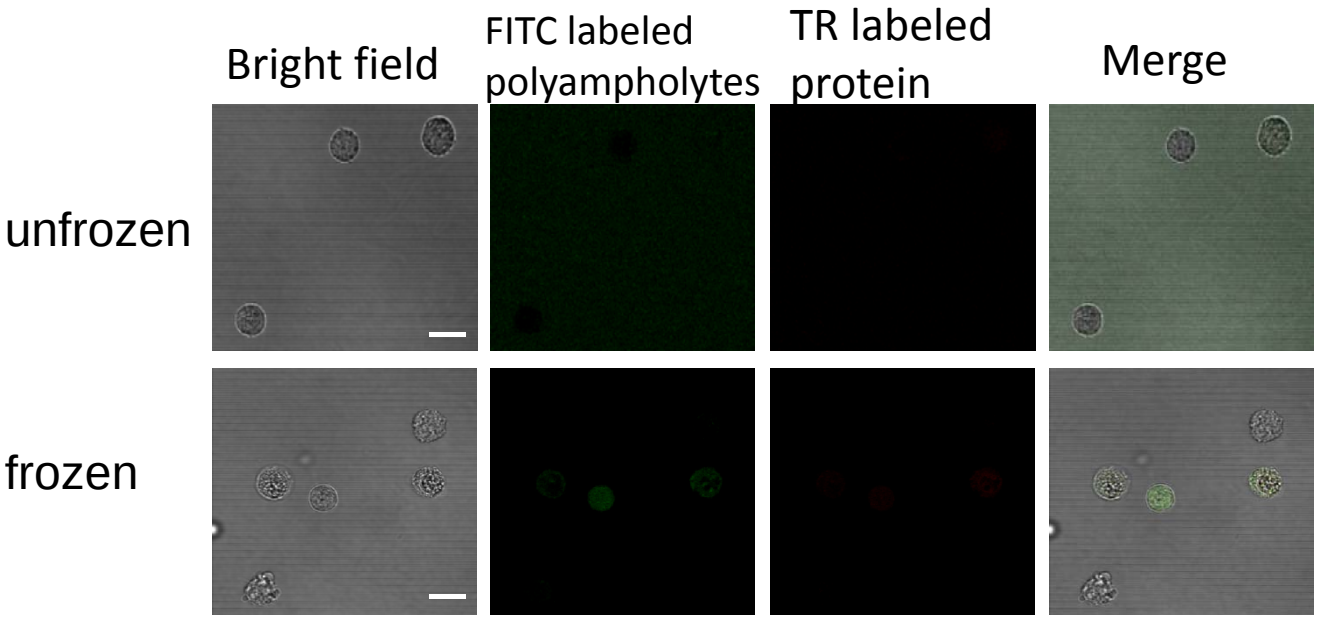

Fig.7(A)

(b) Cells frozen with protein-loaded PLL-DDSA(3)-SA(65)

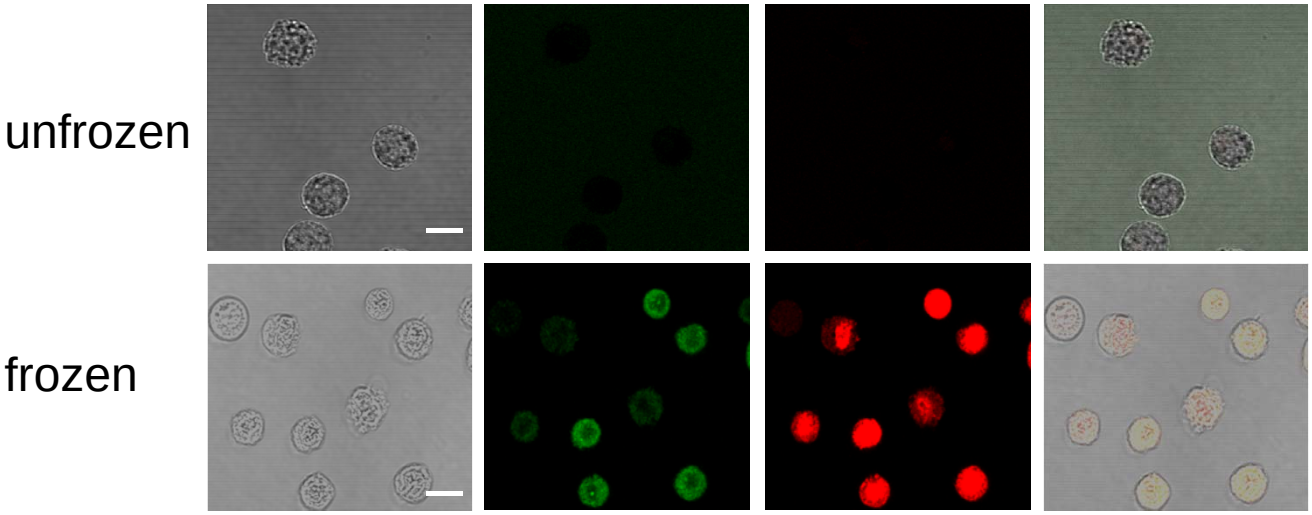

Fig.7(B)

(c) Cells frozen with protein-loaded PLL-DDSA(5)-SA(65)

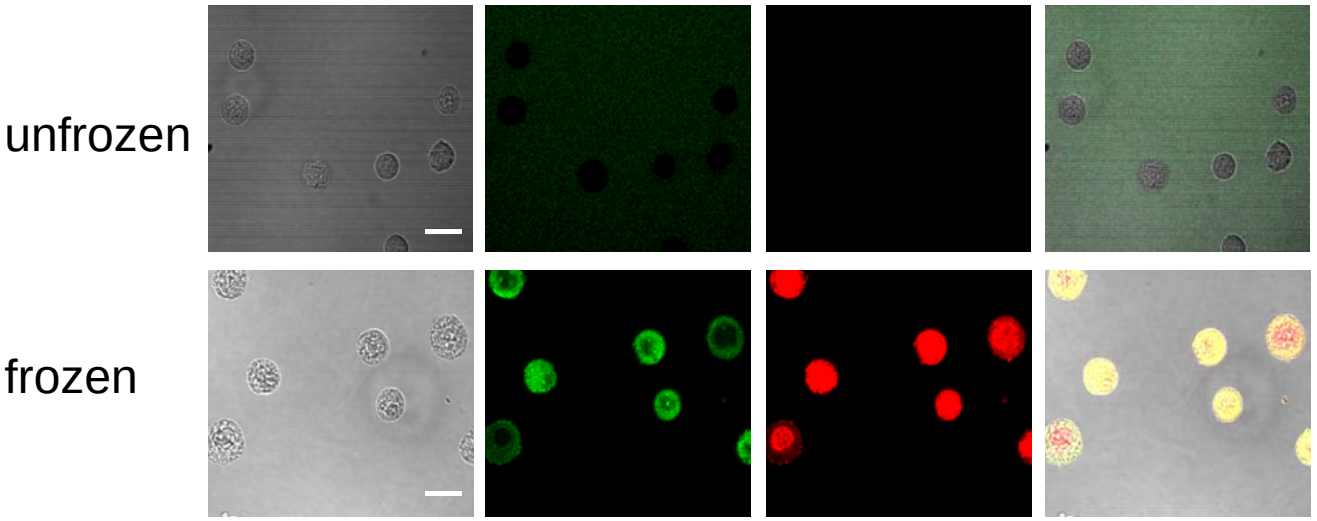

Fig.7(C)

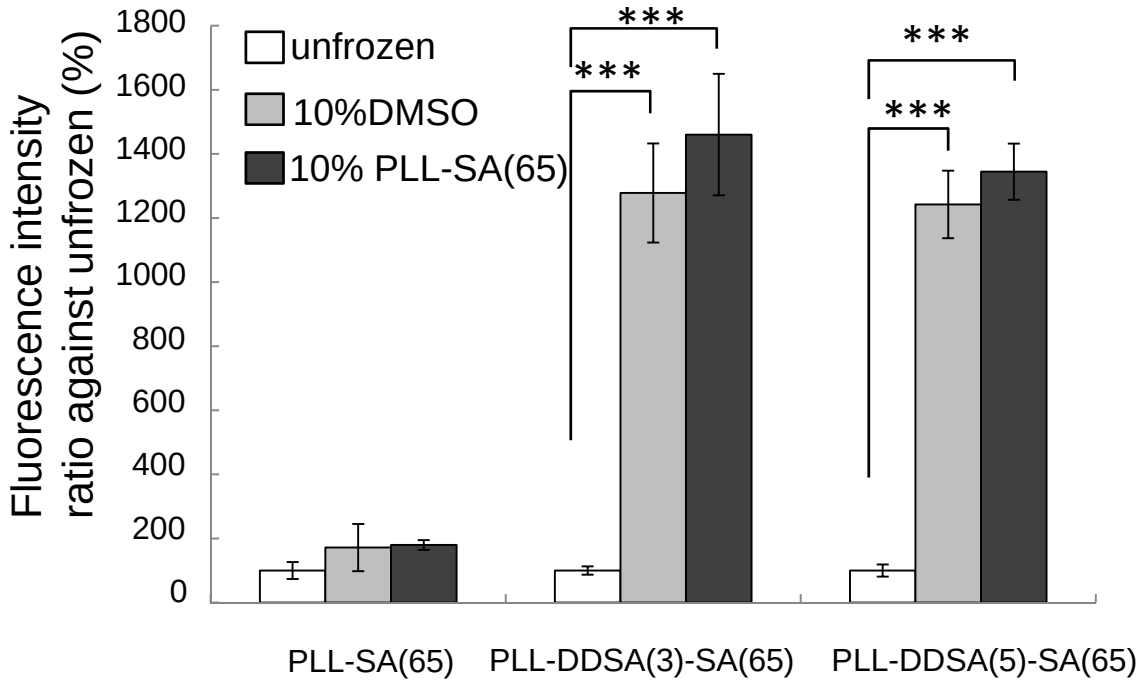
Fluorescence intensity ratio against unfrozen (%)
1800
1600
1400
1200
1000
800
600
400
200
0
unfrozen
10%DMSO
10% PLL-SA(65)
***
***
***
***
PLL-SA(65)
PLL-DDSA(3)-SA(65)
PLL-DDSA(5)-SA(65)

Fig.8

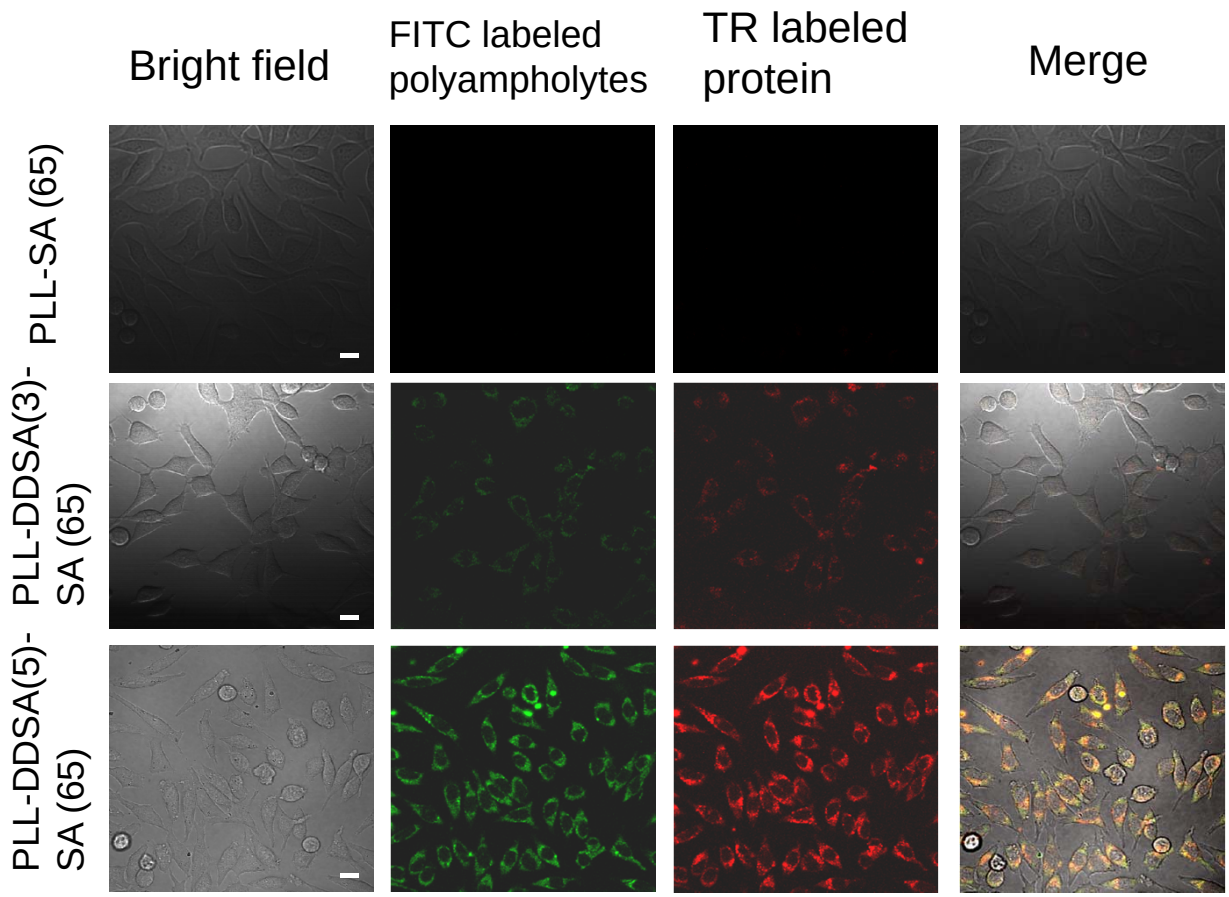
Bright field
FITC labeled polyampholytes
TR labeled protein
Merge
PLL-SA (65)
PLL-DDSA(3)-SA (65)
PLL-DDSA(5)-SA (65)

Fig.9

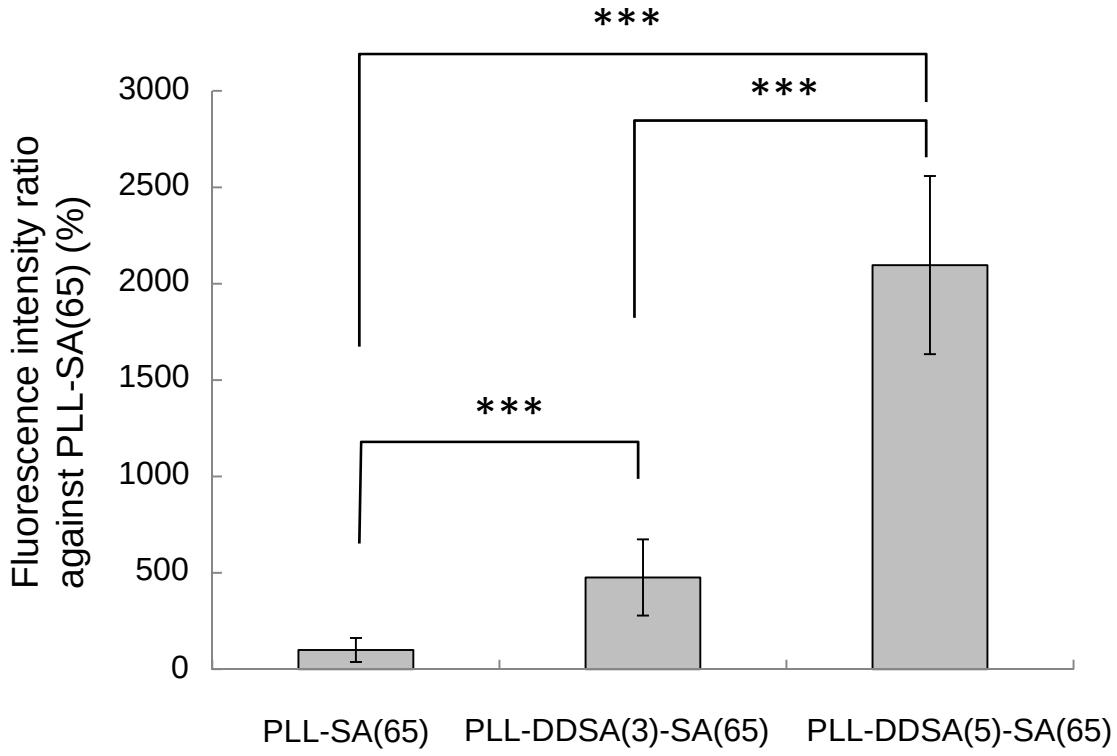
***
***
***
3000
2500
2000
1500
1000
500
0
Fluorescence intensity ratio against PLL-SA(65) (%)
PLL-SA(65)
PLL-DDSA(3)-SA(65)
PLL-DDSA(5)-SA(65)

Fig.10

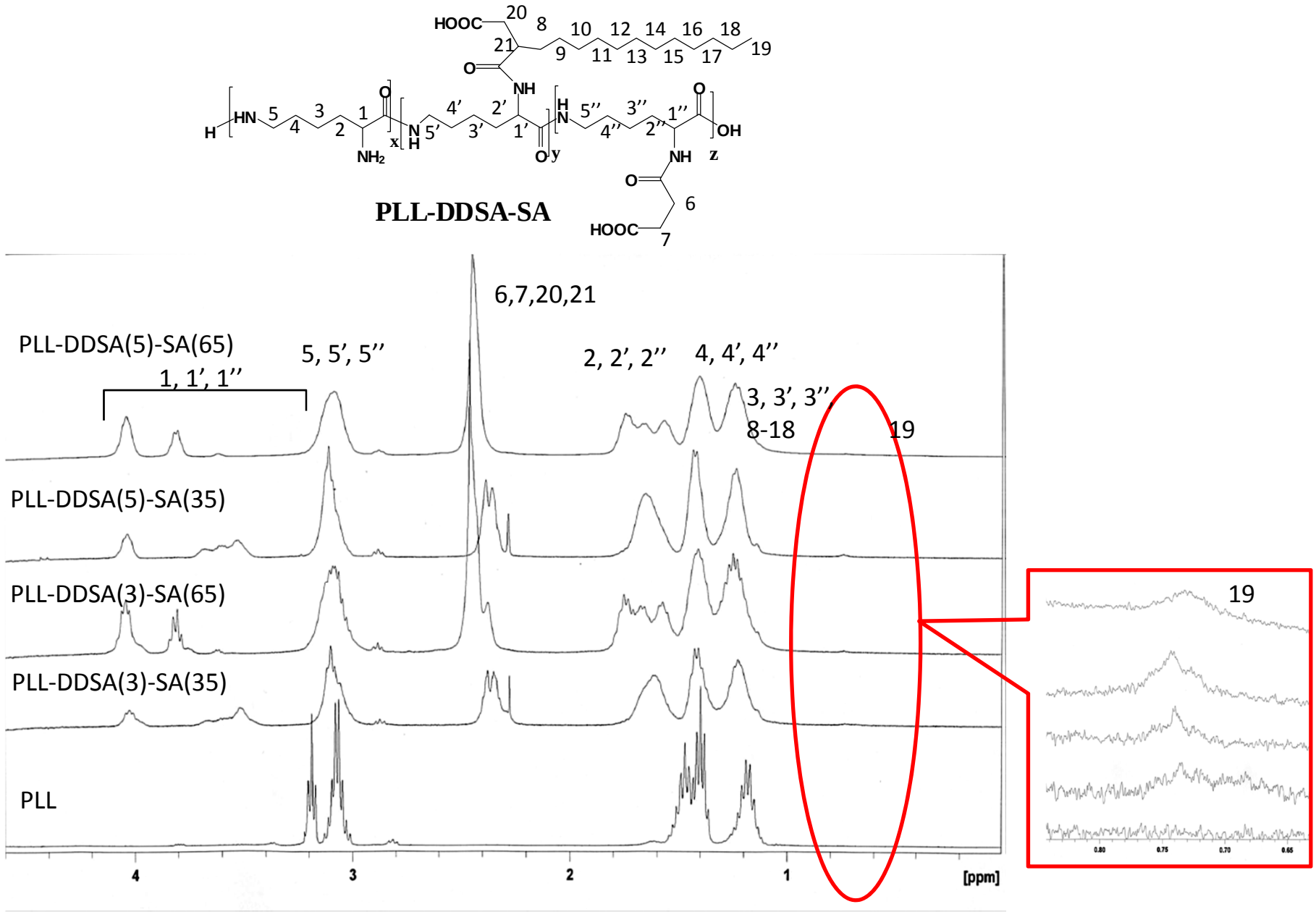
PLL-DDSA-SA
PLL-DDSA(5)-SA(65)
PLL-DDSA(5)-SA(35)
PLL-DDSA(3)-SA(65)
PLL-DDSA(3)-SA(35)
PLL
1, 1', 1''
5, 5', 5''
6,7,20,21
2, 2', 2''
4, 4', 4''
3, 3', 3''
8-18
19
4
3
2
1
[ppm]

Figure S1

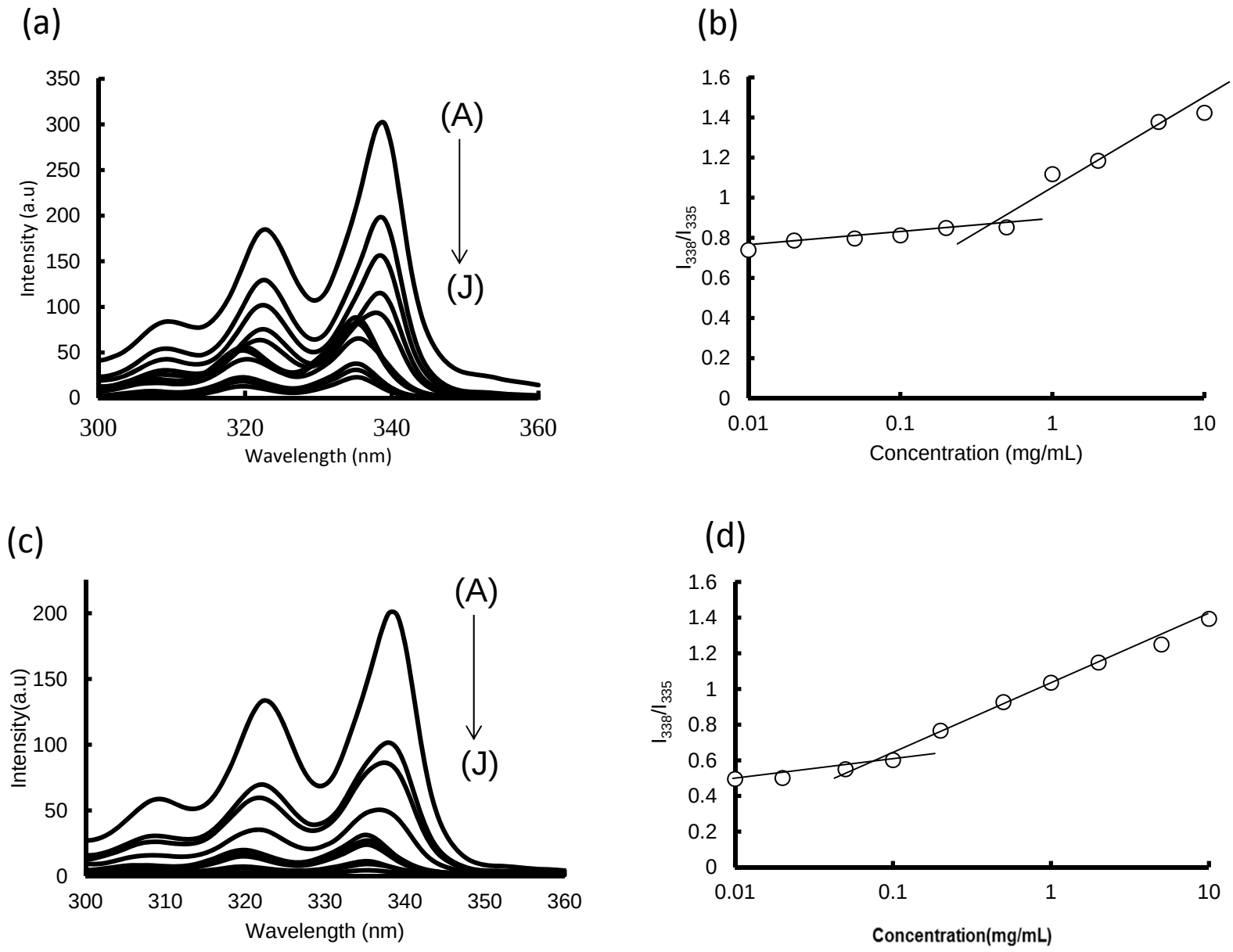
(a)
Intensity (a.u)
Wavelength (nm)
(A)
(J)
(b)
I_{338}/I_{335}
Concentration (mg/mL)
(c)
Intensity(a.u)
Wavelength (nm)
(A)
(J)
(d)
I_{338}/I_{335}
Concentration(mg/mL)

Fig.S2

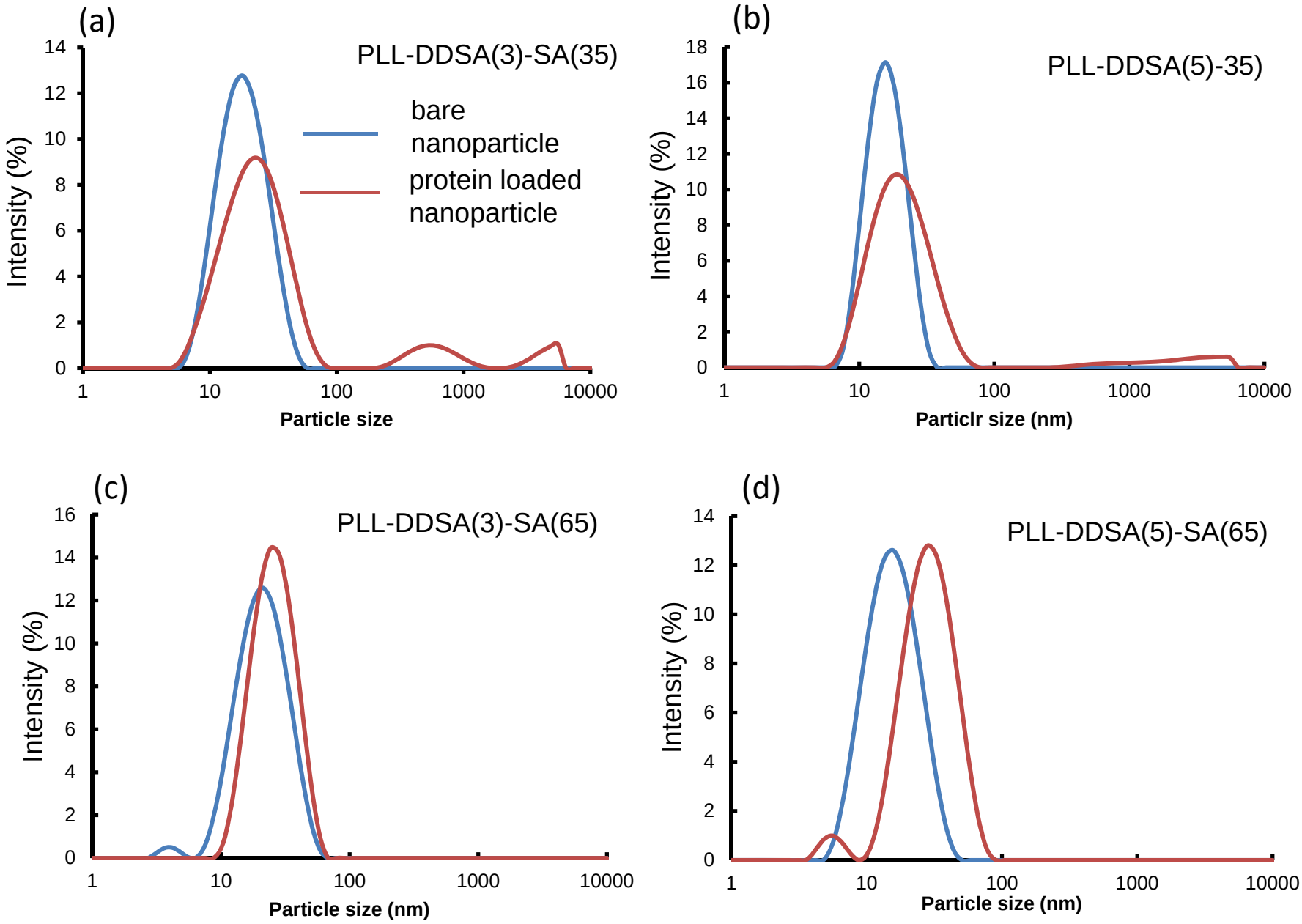
(a)
PLL-DDSA(3)-SA(35)
bare nanoparticle
protein loaded nanoparticle
Intensity (%)
Particle size
(b)
PLL-DDSA(5)-35)
Intensity (%)
Particlr size (nm)
(c)
PLL-DDSA(3)-SA(65)
Intensity (%)
Particle size (nm)
(d)
PLL-DDSA(5)-SA(65)
Intensity (%)
Particle size (nm)

Fig.S3

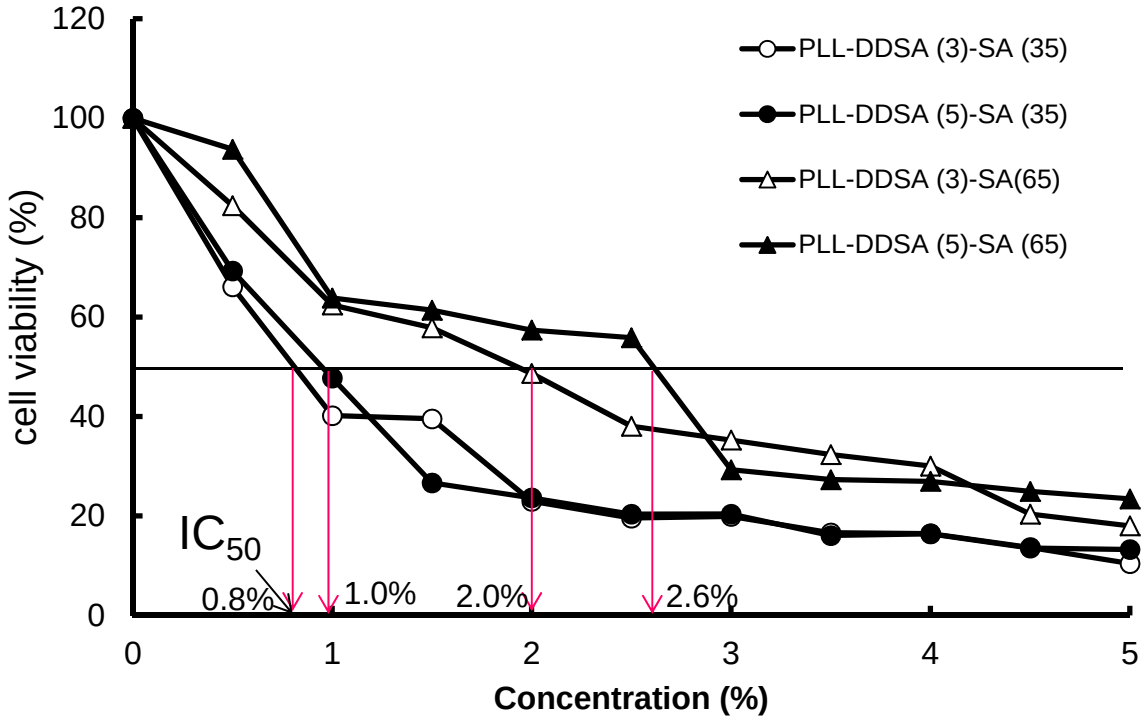
120
100
80
60
40
20
0
cell viability (%)
0
1
2
3
4
5
Concentration (%)
PLL-DDSA (3)-SA (35)
PLL-DDSA (5)-SA (35)
PLL-DDSA (3)-SA(65)
PLL-DDSA (5)-SA (65)
IC50
0.8%
1.0%
2.0%
2.6%

Fig.S4

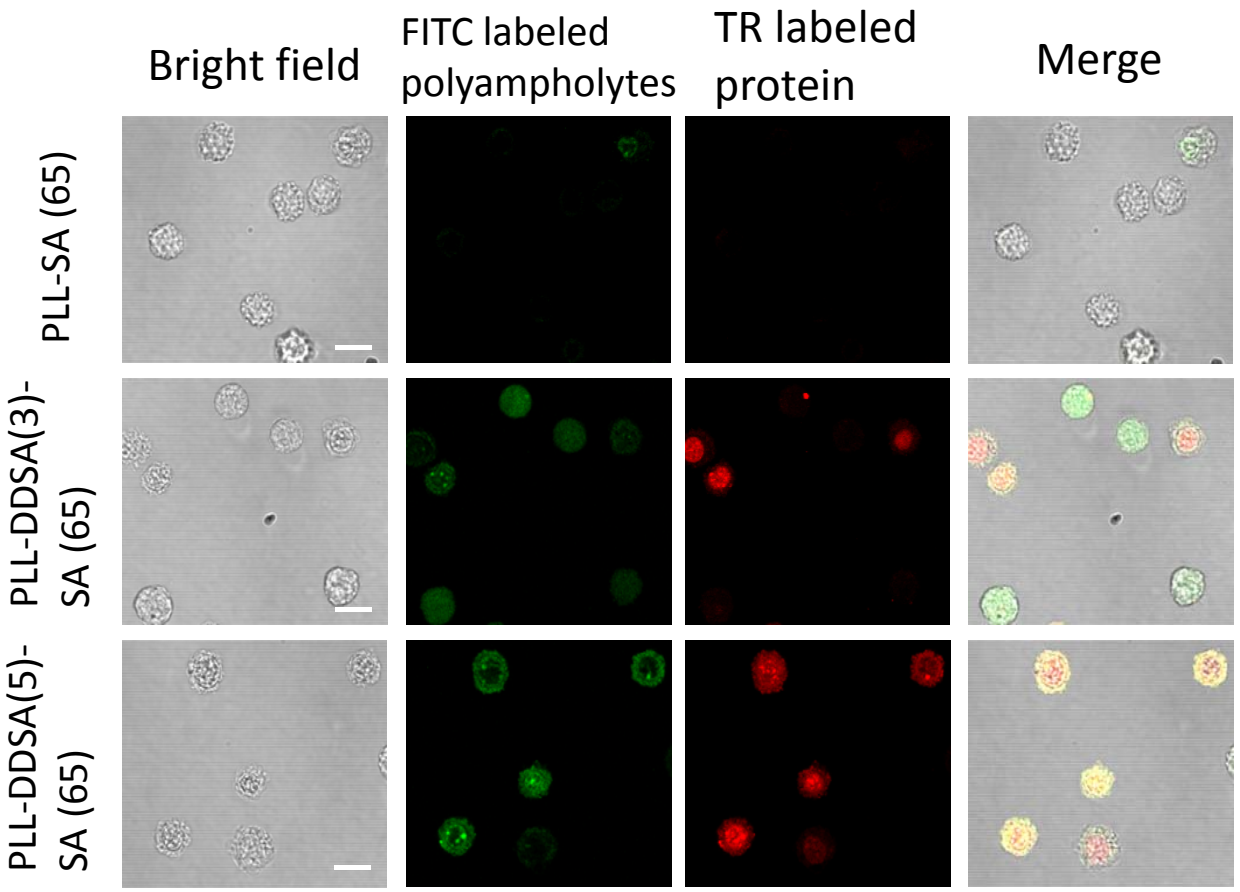
Bright field
FITC labeled polyampholytes
TR labeled protein
Merge
PLL-SA (65)
PLL-DDSA(3)-SA (65)
PLL-DDSA(5)-SA (65)

Fig.S5

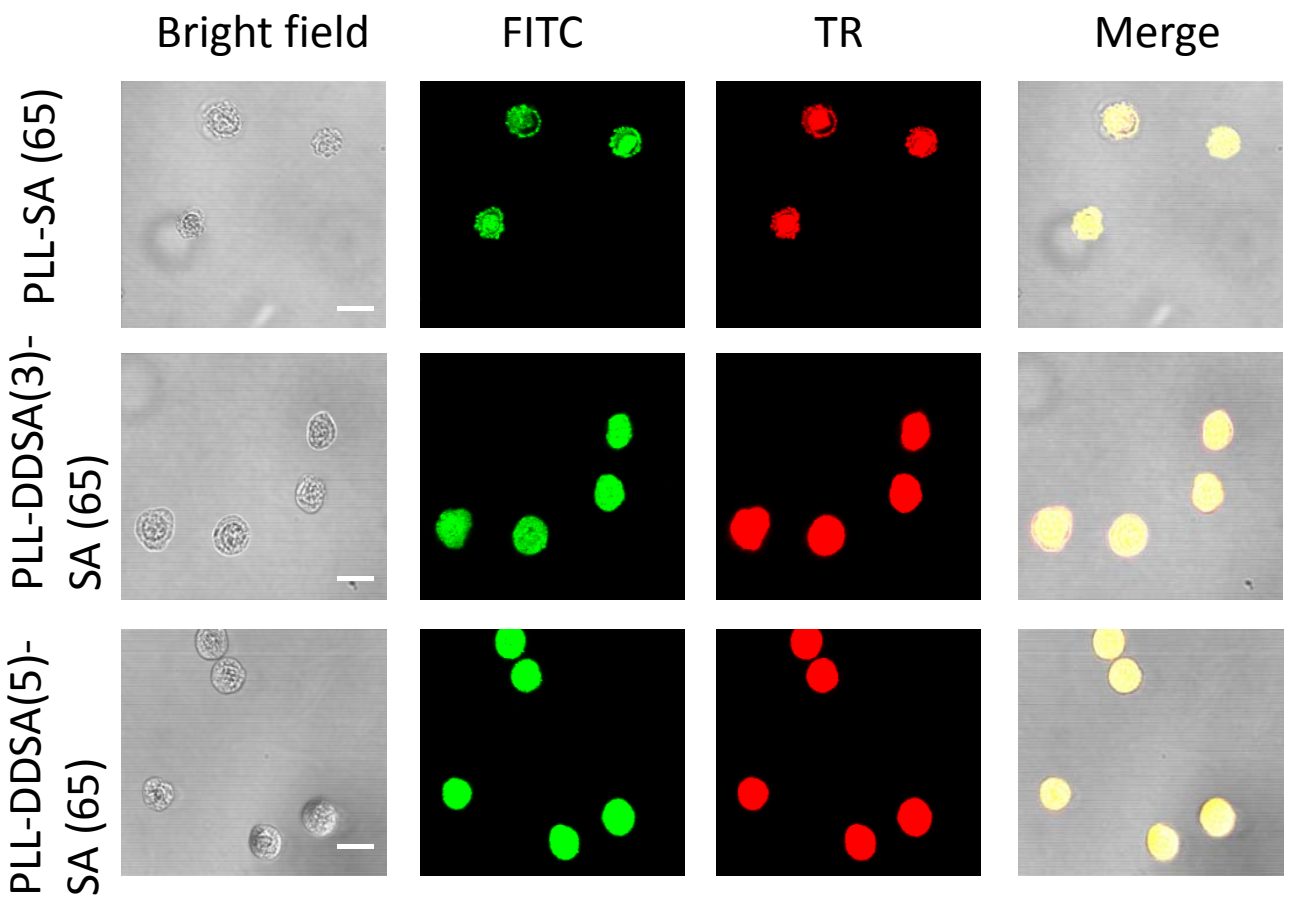
Bright field
FITC
TR
Merge
PLL-SA (65)
PLL-DDSA(3)-SA (65)
PLL-DDSA(5)-SA (65)

Fig.S6

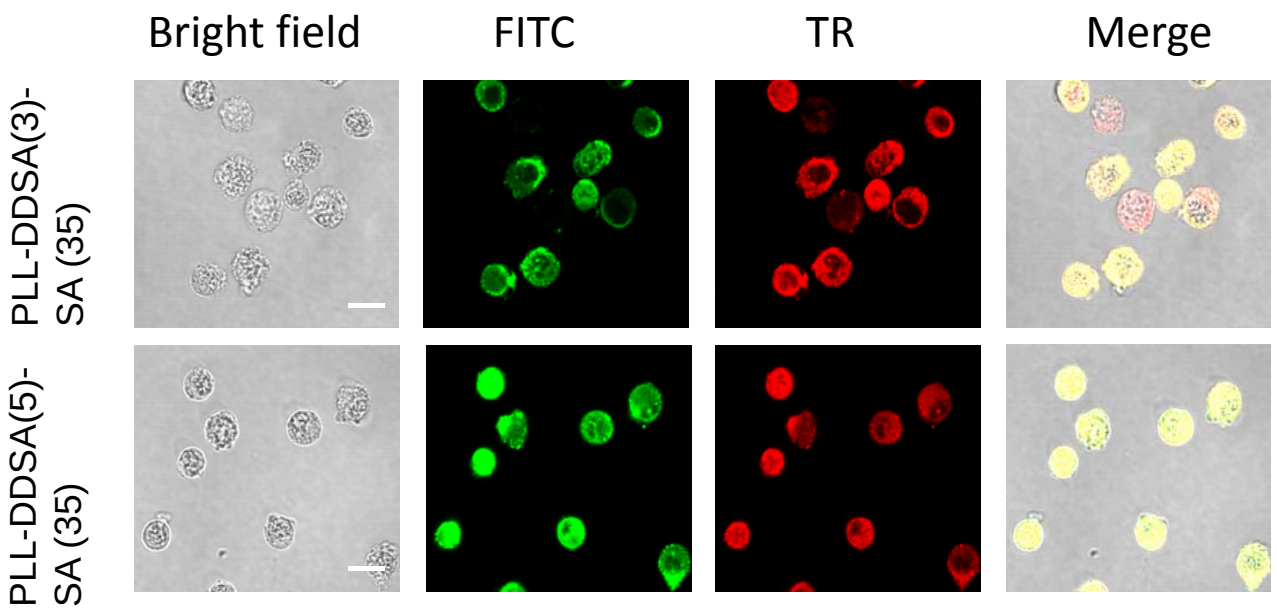

Fig.S7

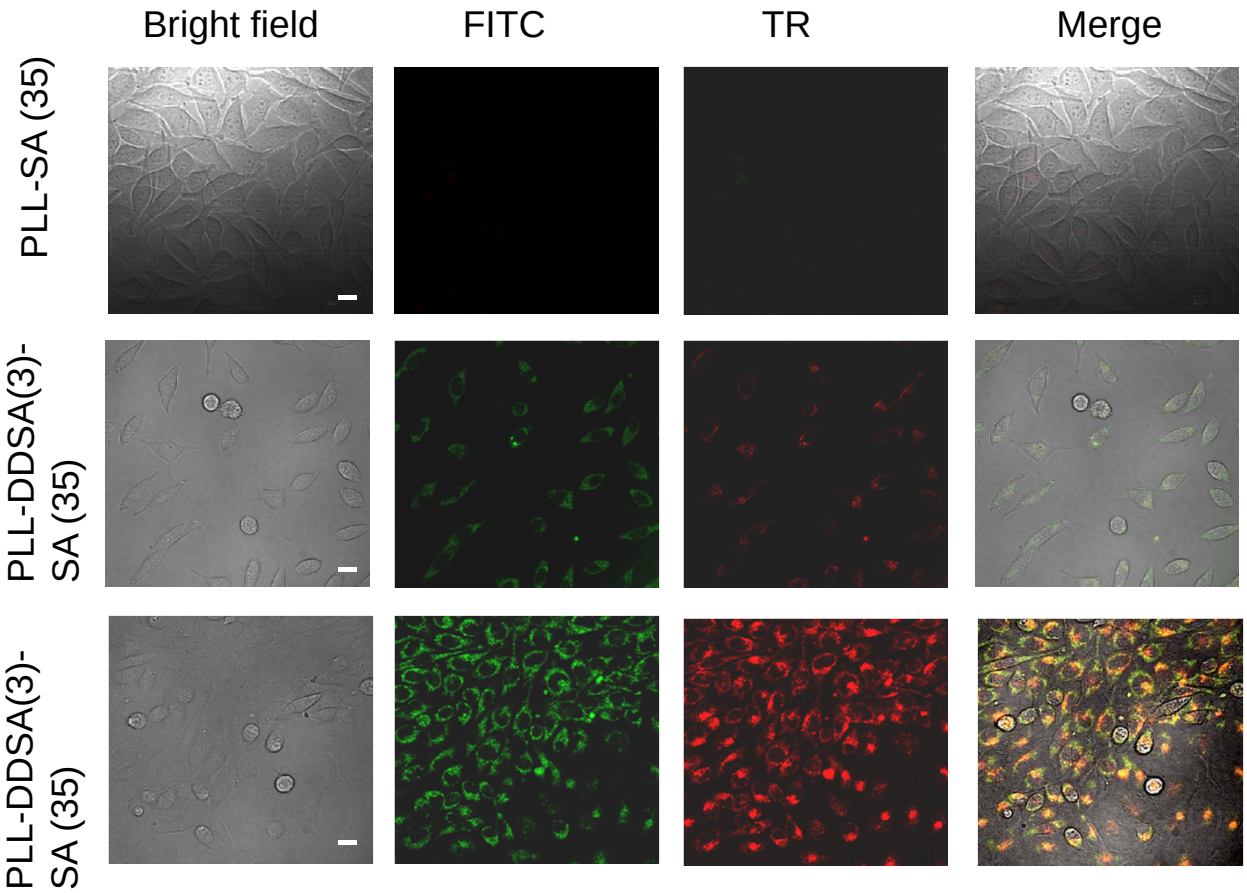
Bright field
FITC
TR
Merge
PLL-SA (35)
PLL-DDSA(3)-SA (35)
PLL-DDSA(3)-SA (35)

Fig.S8

Supplemental data

Enhanced Protein Cytoplasmic Delivery using Polyampholyte Nanoparticles and the Freeze Concentration Mechanism

Sana Ahmed, Fumiaki Hayashi, Toshio Nagashima, and Kazuaki Matsumura*

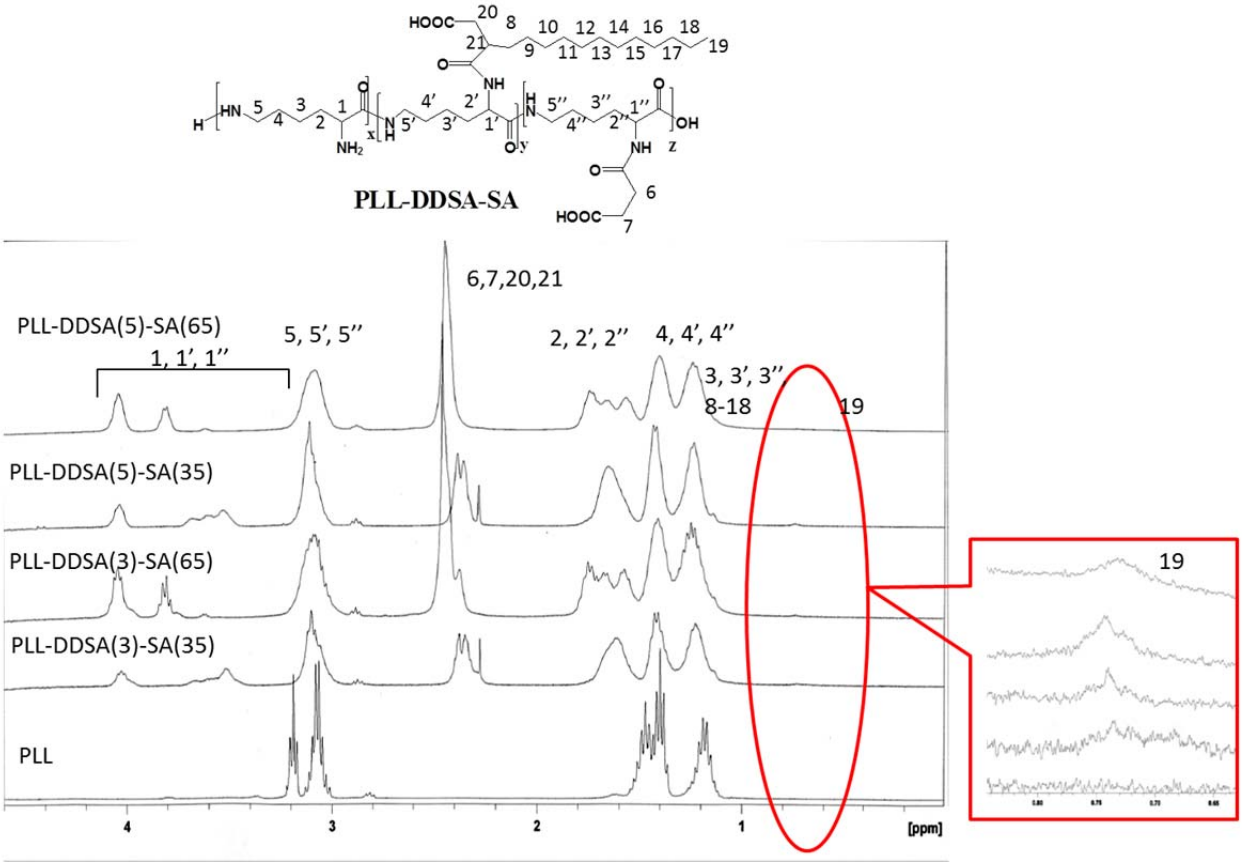

Figure S1. ^{1}H-NMR spectra of hydrophobically modified polyampholytes and intact PLL.

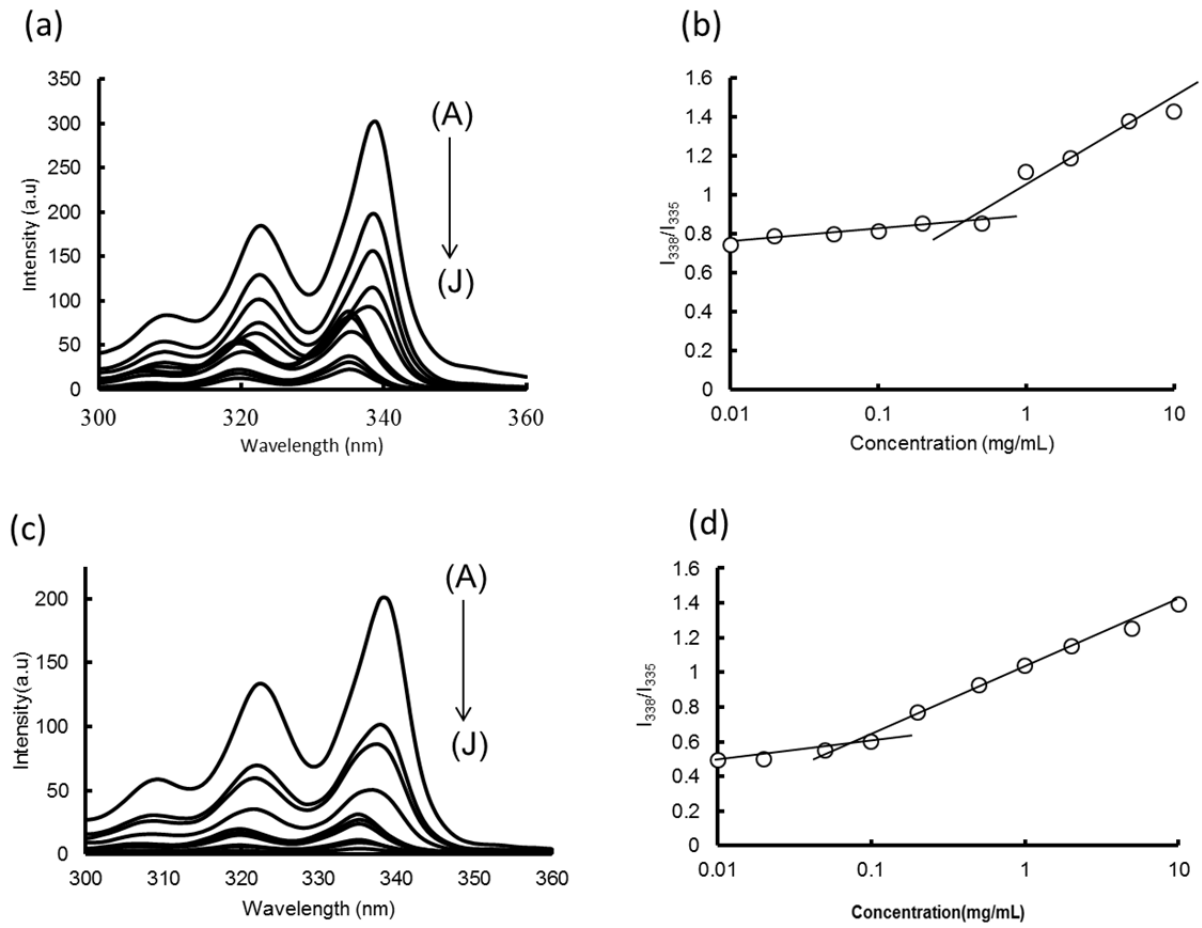

Figure S2. Determination of the CACs of different nanoparticles. Excitation spectra of pyrene of (a) PLL-DDSA(3)-SA(35) and (c) PLL-DDSA(5)-SA(35) solutions of different concentrations (a-j) 10, 5, 2, 1, 0.5, 0.2, 0.1, 0.05, 0.02, and 0.01 mg/mL, respectively. Plot of the ratio of I_{338}/I_{335} against the logarithm of the concentration of (b) PLL-DDSA(3)-SA(35) and (d) PLL-DDSA(5)-SA(35).

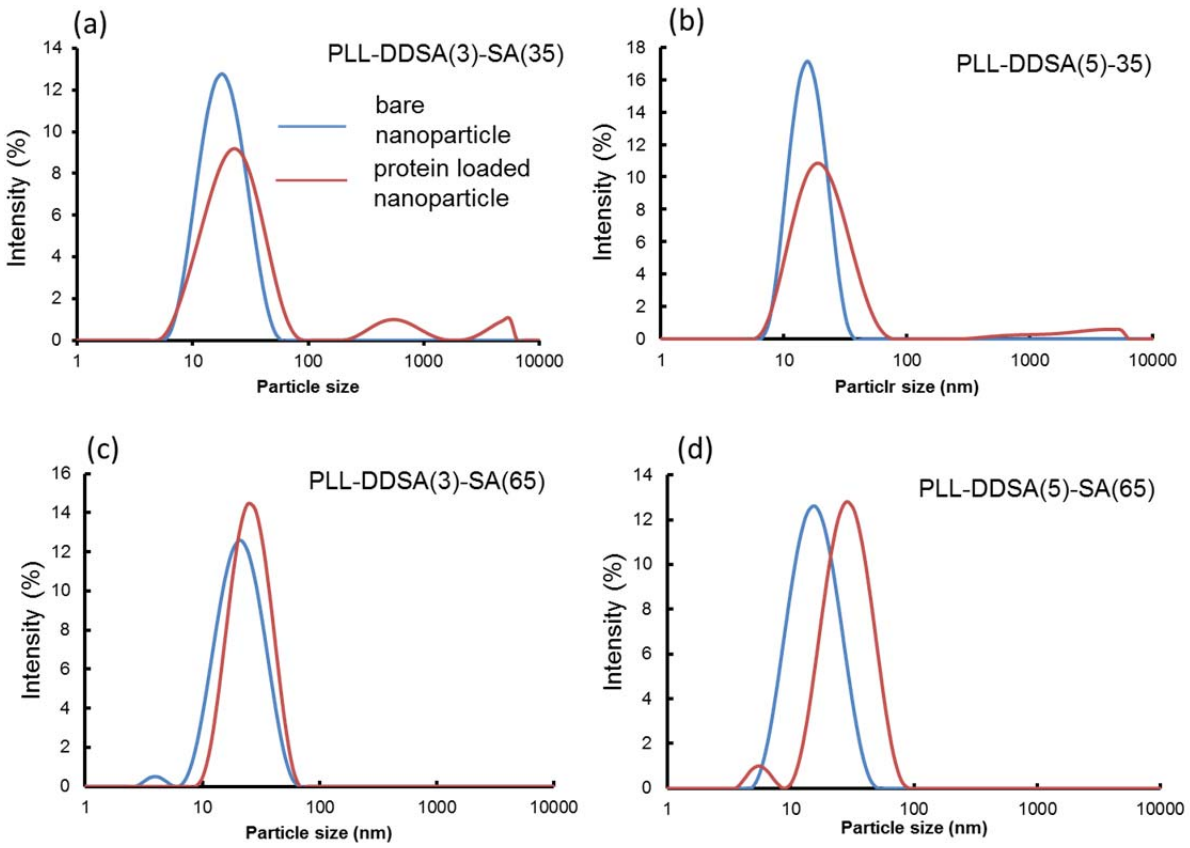

Figure S3. Size distribution of polyampholyte nanoparticles before and after protein adsorption.

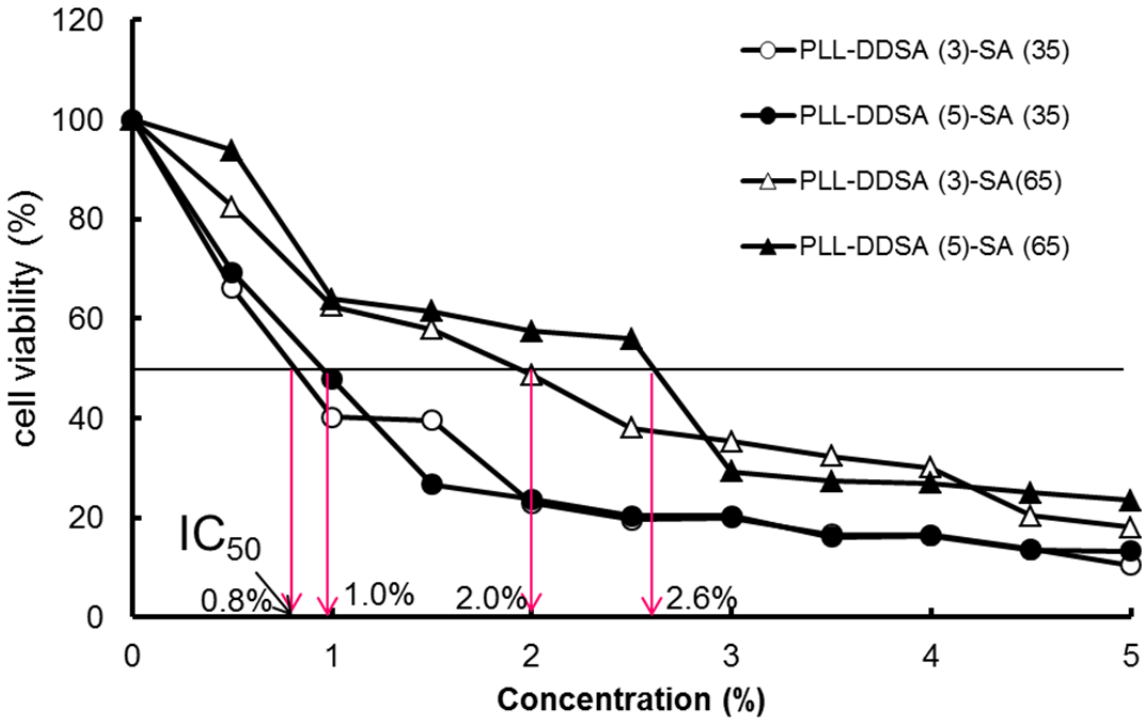

Figure S4. Cytotoxicity of nanoparticles. L929 cells were incubated with the indicated concentration of nanoparticles for 48 h, followed by the MTT assay. Data are described as the percentage of untreated cells. Mean values and standard deviations for independent triplicate experiments (8 samples each) are shown. IC_{50} represents the concentration of nanoparticles that caused a 50% reduction in MTT uptake by a treated cell culture compared with the untreated control culture.

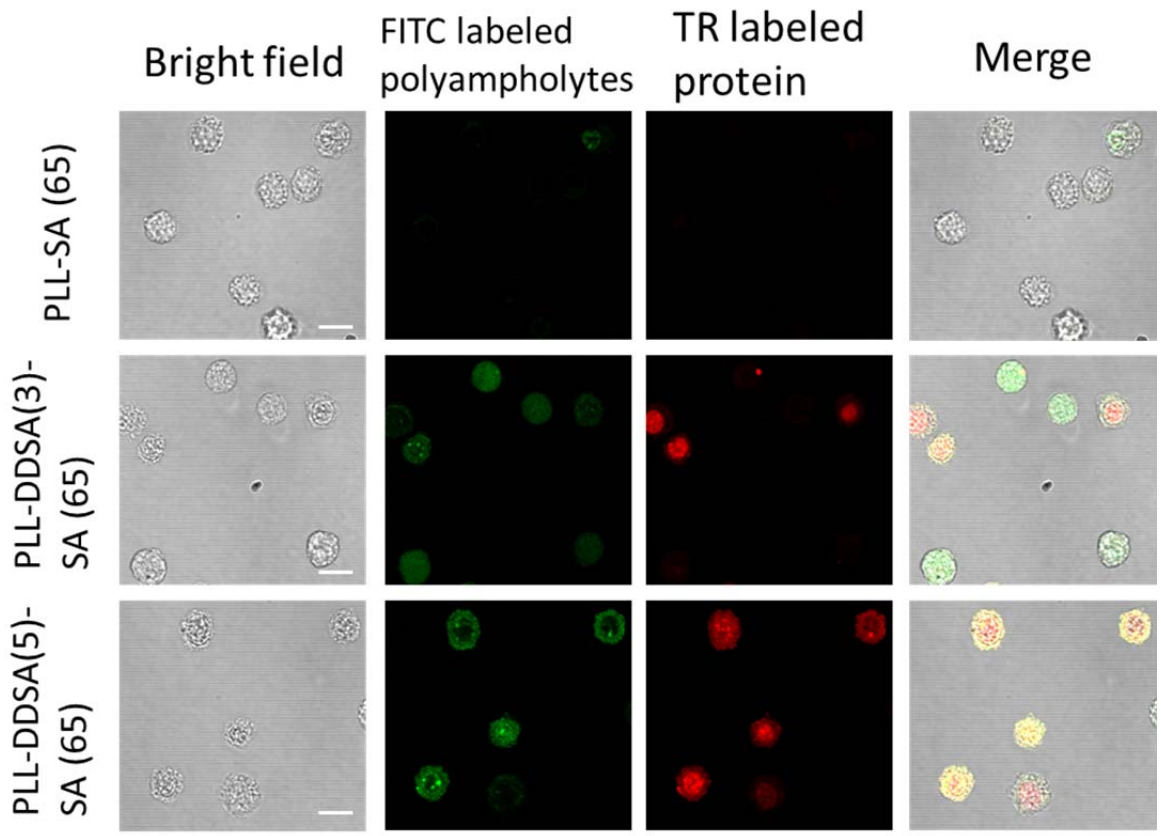

Figure S5. Confocal microphotographs of L929 cells after freezing with various protein-loaded polyampholyte nanoparticles with 10% DMSO as a cryoprotectant. The bars: 10μm.

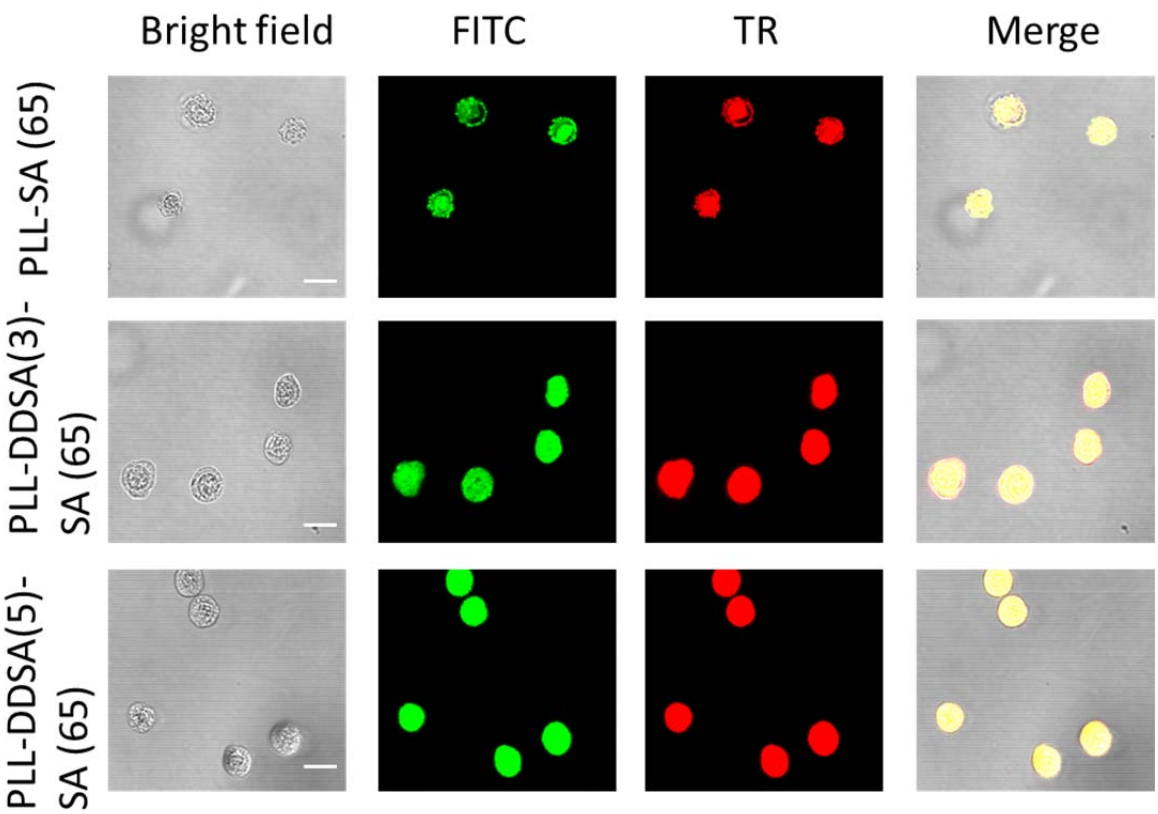

Figure S6. Confocal microphotographs of L929 cells after freezing with various protein-loaded polyampholyte nanoparticles without a cryoprotectant. No cells survived and a high fluorescence was observed because of cell membrane rupture. The bars: 10μm.

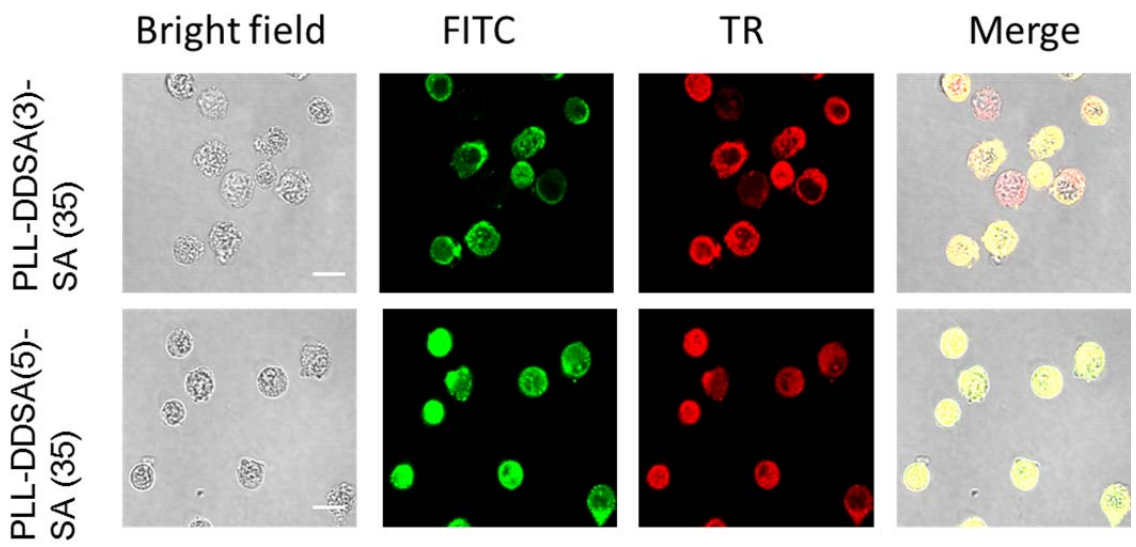

Figure S7. Confocal microphotographs of L929 cells after freezing with various BSA-loaded PLL-DDSA(3 or 5)-SA(65) nanoparticles with 10% PLL-SA(65) as a cryoprotectant. The bars: 10μm.

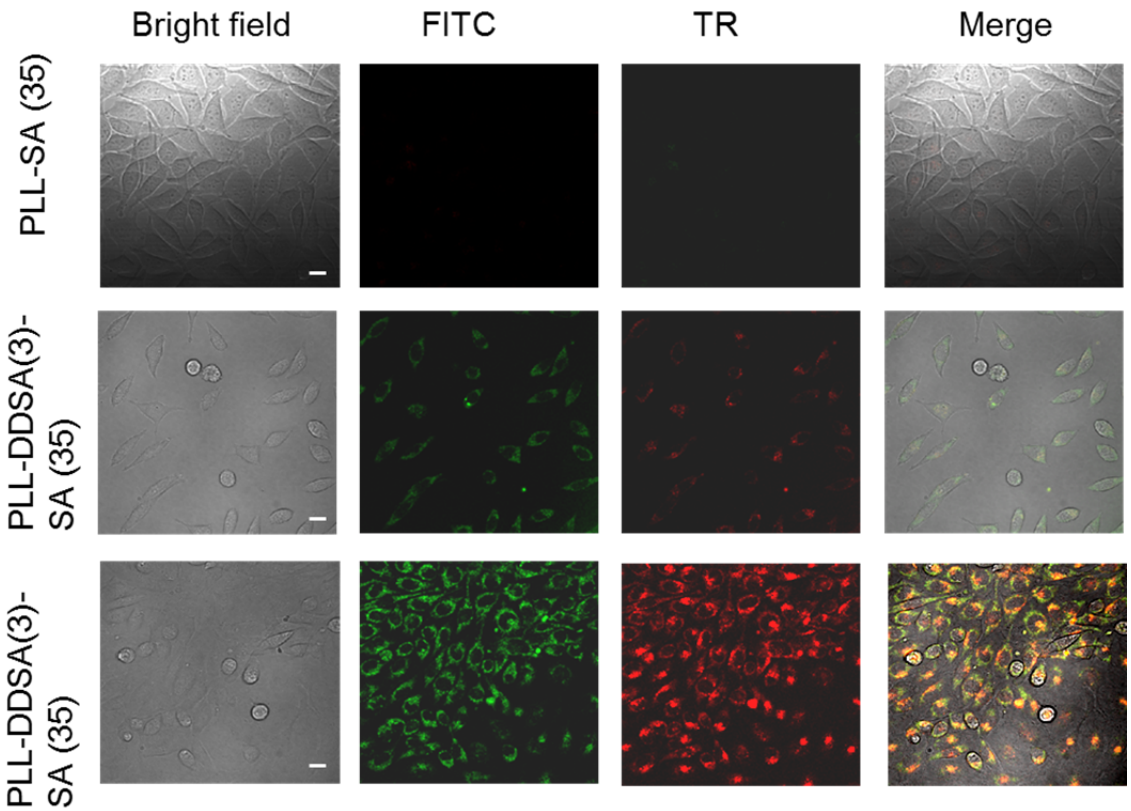

Figure S8. Protein internalization via endocytosis during culture after being frozen with BSA and PLL-(SA) and BSA-loaded PLL-DDSA(3 or 5)-SA(35) nanoparticles with 10% PLL-SA(65) as a cryoprotectant. The bars: 10μm.